Washington University in St. Louis

James McKelvey School of Engineering

Final Report for MEMS 598 Energy Analysis and Design Project

Performance Characterization of a Novel Thermal-Fluid Exchange between an Electric Vehicle and a DC Charging Station

By: Matthew Celentano

Report Date: December 29, 2020

1 Abstract

This paper discusses a new approach to Electric Vehicle (EV) charging through the use of a thermal-fluid exchange between the vehicle and the charging station. Charge times that are longer than those required by combustion engines reduce the viability of EVs among consumers. In this battery thermal management system, a liquid-cooled charging cable is used to provide both electricity and coolant flow between the vehicle and the charging station. A Simulink simulation is used to model the system across a range of ambient temperatures and voltage architectures. Ambient temperature is varied from 0° C to 37° C and voltages between 400 V and 800 V are tested. Simscape is used to model the thermal, electrical, and fluid systems. The use of an organic Rankine cycle is also explored. The simulation results show that the system is capable of charging a vehicle from 0% to 100% in 255 seconds while keeping battery temperature and wire temperature within a safe range. Through four experiments, the maximum battery cell temperature is found to be 39° C and the maximum wire temperature is 50° C when using an 800 V architecture with a maximum Rankine cycle efficiency of 18%.

Contents

2 Introduction

In recent years, the automotive industry has experienced a shift toward the electrification of vehicles. The impetus of this shift is due to a variety of factors; including concerns about climate change, advances in battery technology, and a psychographic change in the consumer. There are, however, significant downsides to electric vehicles (EVs) compared to their internal combustion engine (ICE) counterparts. These downsides include high production costs, short battery range, and slow charging speed. This research explores a new method of high-speed direct current (DC) charging with an aim to eliminate the current downside of charging speed.

The Society of Automotive Engineers (SAE) has defined 3 levels of charging for EVs. Level 1 and 2 are alternating current (AC) charging standards most useful for home and work charging. Level 3 charging, however, is a DC standard aimed at providing much higher charging rates [1]. This third standard is the focus of this research as it is currently the limiting factor in long-distance transportation. Current level 3 charge rates are limited to between 50-350 kW. At 350 kW, the Porsche Taycan can extend its range by 85 miles in 10 minutes [2]. On the other hand, the Chevrolet Bolt, which charges at 50 kW is capable of charging at a rate of 30 miles in 10 minutes [3]. In contrast, ICE vehicles can refuel at a rate of 300 miles in about 4 minutes. To make EVs more compelling to the consumer, the rate of charge must be increased significantly above its current levels.

There are two main limitations that bottleneck current charge rates. One limitation is the fundamental electro-chemistry of lithium-ion cells. The other is the thermal limitation in extracting heat out of the battery during the charging process. This research takes electro-chemistry as a given and focuses on optimizing the heat transfer process. As such, the charge rate was set to the maximum commercially available charge rate of 15C for a lithium-ion battery [4]. For reference, 1C means that a battery can charge from 0-100% in 1 hour. A rate of 15C indicates that a battery can charge from 0-100% in 4 minutes.

Heat is generated during charging through both the charging cable and the battery. The heat generated through the cable is a function of its resistance and temperature. The heat generated in a lithium-ion cell is a function of the internal resistance in that cell. As the cell is charged, a current flows through the battery generating heat through a resistance that is a function of the cell temperature. Existing research has determined that an appropriate approximation for the heat generated by a battery cell is found when using a two RC-branch equivalent circuit. This circuit is comprised of two resistance-capacitor circuits in series [5]. Both the resistance and capacitance are a function of the internal temperature of the cell. As the temperature increases, the resistance increases, further increasing the temperature of the cell. This positive feedback relationship can cause a thermal-runaway event in which the separation layers in the battery melt which creates a short circuit, leading to a fire. Electro-chemical limitations create a narrow optimal temperature window between 20°-40° C [6]. Cell temperatures outside this range can lead to sub-optimal battery degradation over time. This research aims at creating a thermal network to maintain this temperature range at high rates of charge.

There are two ways that EV battery temperature are currently regulated. In a passively cooled battery pack, heat is extracted out of the battery through natural convection between the pack and the atmosphere. This is the case with vehicles such as the Nissan Leaf [6]. Active cooling is achieved by pumping a thermal-fluid, typically consisting of a mixture of ethylene glycol and water, through the battery pack by forced convection between the battery cells and the thermal-fluid. This thermal-fluid is cooled with a radiator which exchanges heat with the atmosphere. Most automakers such as Tesla, General Motors, Ford, and VW use this active method to cool the batteries during charging due to its higher inherent heat transfer rate [6]. These active system are limited by the size of the vehicle's radiator, coolant volume, and pump power, due to vehicle packaging and weight constraints.

This research introduces a new form of active cooling that eliminates the limitations outlined above. It consists of a thermal-fluid exchange between the EV and a DC

charging station. A pump in the charging station forces fluid into the battery through a charging cable with a liquid jacket exterior. The cross-section of the cable is shown in Figure 1.

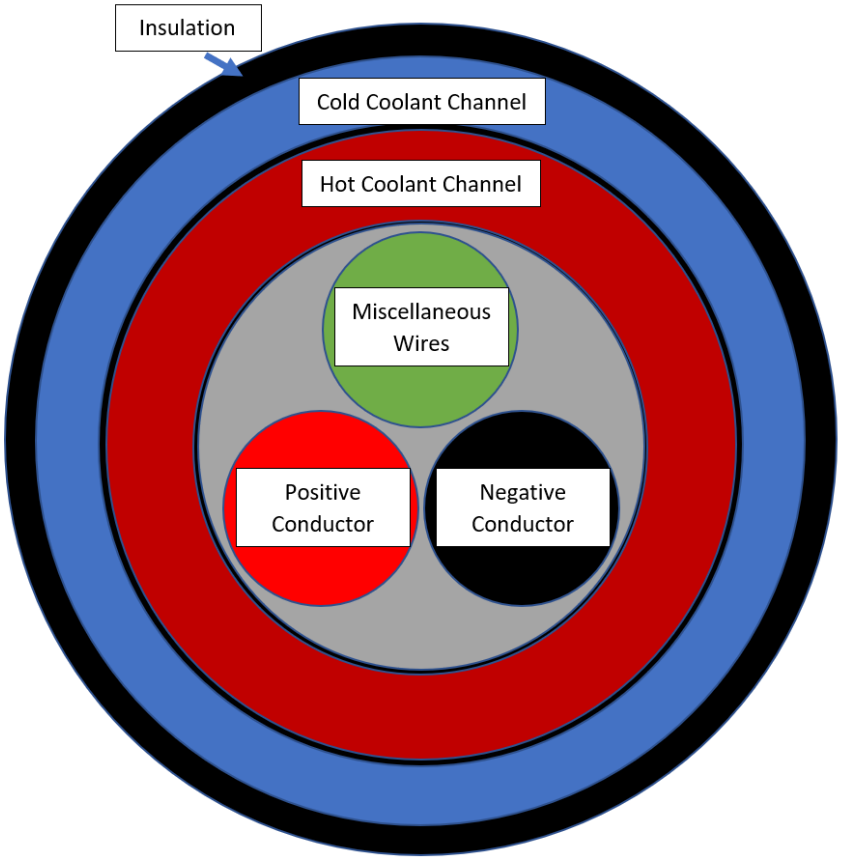

Figure 1: Cross section of charging and cooling wire

This fluid flows through the battery pack, rapidly extracting heat out of the battery. It then travels back through the charging cable where it flows into a reservoir. The heat can be removed from the fluid in a variety of ways. It can be dissipated through a geothermal exchange between the fluid and bedrock, through an exchange between the fluid and the atmosphere, or through using an additional organic Rankine cycle that can use some of the heat energy to generate electricity. The schematic for this system is shown in Figure 2.

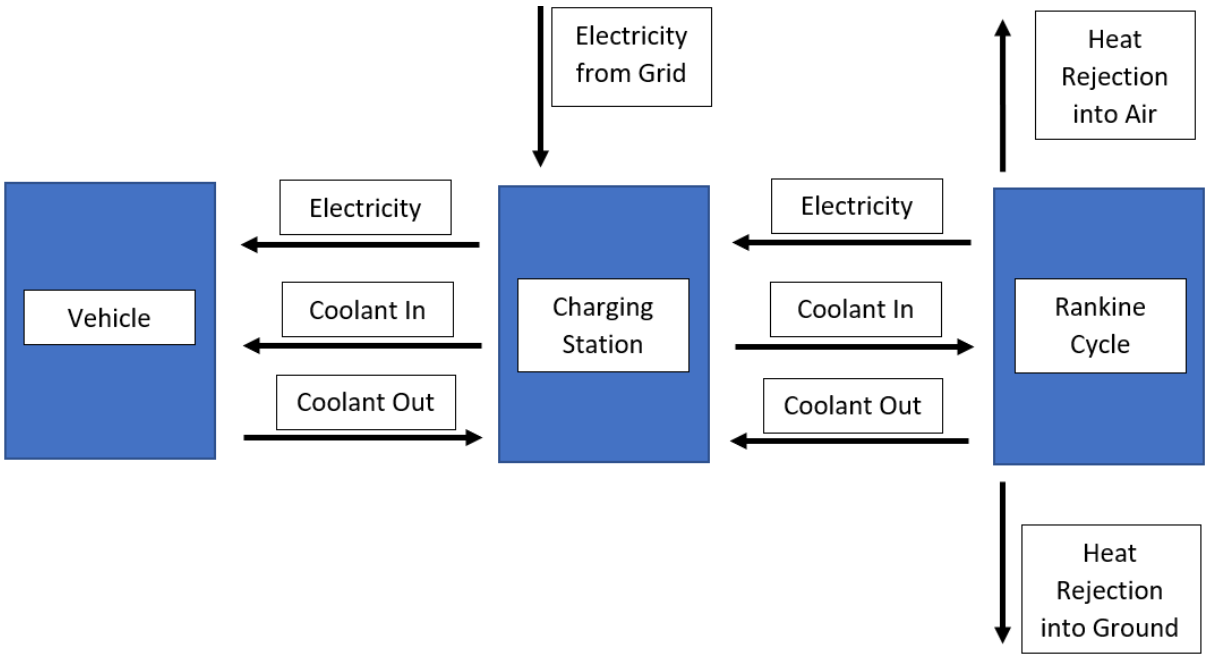

Figure 2: System schematic with electricity and heat flows

The organic Rankine cycle is a two-phase cycle which uses a refrigerant as the working fluid. Refrigerants are used to lower the evaporation temperature below the maximum expected temperature of the system. For example, in this research, the maximum temperature of the system is 40° C, as this is the maximum safe battery temperature. Accordingly, a working fluid must be selected with an evaporation temperature below this maximum. The Rankine Cycle works in the following stages. In the first stage, the liquid working fluid is pumped from low pressure to high pressure through isentropic compression. In the second phase, the working fluid is evaporated in a heat exchanger connected to the high-temperature source through an isobaric process. In the third phase, The working fluid vapor expands through a turbine which rotates a shaft (this shaft is connected to a motor that generates electricity) through isentropic expansion. The working fluid is a mixture of a fluid and a vapor at this point. In the last phase, the fluid is cooled through a condenser through an isobaric process.

This research optimizes the thermal exchange between the battery cell, charge cable, organic Rankine cycle, and atmospheric/geothermal heat rejection through a system-level computer simulation model. The next section outlines the methods, constraints, and

assumptions used to make this model.

3 Methods

3.1 Assumptions, Constraints, and Software Setup

The system size is set to cool a 100 kWh battery pack. This is the largest battery pack available in a vehicle today. Furthermore, 18650 cylindrical battery cells are used in this analysis as they are the most popular cells found in EV battery packs [7]. The cells are assumed to have a uniform temperature throughout and are simplified using a 2-RC equivalent circuit.

Throughout the modeling process, the system is considered ideal to reduce complexity in the model. Moreover, various analytical and empirical relationships are used to simplify actual heat transfer behavior. The modeling is constrained to a single vehicle although the costs of the system would be reduced if multiple vehicles were connected to the same thermal network. Since this system is considered to be ideal, the final results can be multiplied by the number of desired vehicles to find the total performance for a given charging station.

MathWorks' Simulink, an add-in available for MATLAB, is used to run the system-level analysis [8]. Simulink is a signal processing software package used to model and simulate dynamic systems. Simulink uses blocks to represent each part of a system. The blocks are a function that receives an input signal and transforms that signal which is output into the system. These blocks are connected in a dynamic network that updates the input to each block over time. Simscape, a tool within Simulink, is used to model physical systems through a library of electrical, mechanical, fluid, and heat blocks. Together, Simulink and Simscape are used to model the system and run the simulation on the system. The time step for the simulation is set to 0.001 seconds and the length of the simulation is dependent on the state of charge (SOC) of the battery cell.

3.2 Battery Cell Model

The 2RC lithium cell is adapted from T. Huria et al. "High Fidelity Electrical Model with Thermal Dependence for Characterization and Simulation of High Power Lithium Battery Cells," [5] as this battery model is included in the MATLAB library. The 3.6 V cell in this model is relatively uncharged. The following changes are made to represent a 18650 lithium-ion cell. The initial SOC is set to 0% and the cell thermal mass is set to 45 g to represent the average weight of a 18650 cell. The Simscape charging model is shown below.

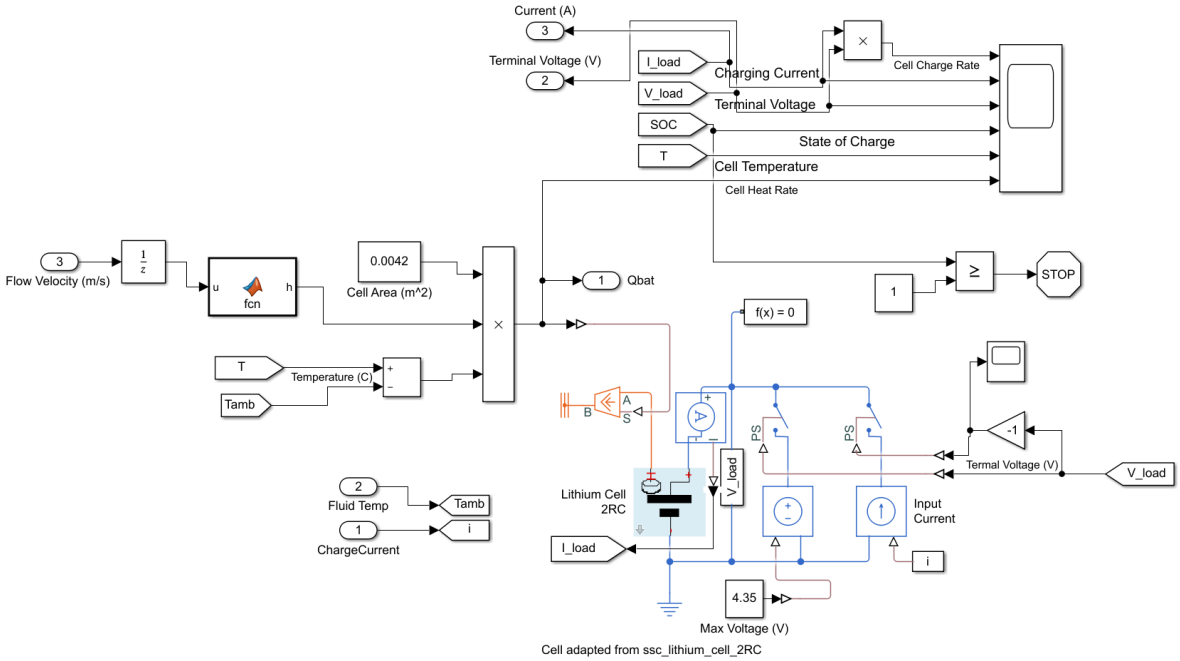

Figure 3: Simscape cell-level model

To prevent excess heat generation in the battery throughout the charging process, the current and voltage are regulated in what is known as a Constant Current Constant Voltage (CCCV) charging scheme. For a 3.6 V cell, the current is held constant until the terminal voltage reaches 4.35 V, the maximum voltage of a 3.6 V lithium-ion cell. At this point, the circuit switches to a constant voltage configuration in which the current is modulated to maintain 4.35 V. The cell continues to charge until it reaches a 100% SOC at which point the simulation ends. The input current is set at the system-level and

divided by the number of the cells in the pack. For a 100 kWh pack, the input current is divided by 7716 cells. The charge rate is set at 54 W per cell. At this high charge rate, there is a significant amount of heat generated in the battery that is extracted through the thermal model.

The thermal model for the battery consists of forced convective heat transfer between the battery cell and the thermal network. The cell area in contact with the thermal-fluid is assumed to be the cylindrical part of the surface of the cylinder. The fluid flows past the cylinder in a cross-flow configuration, shown below.

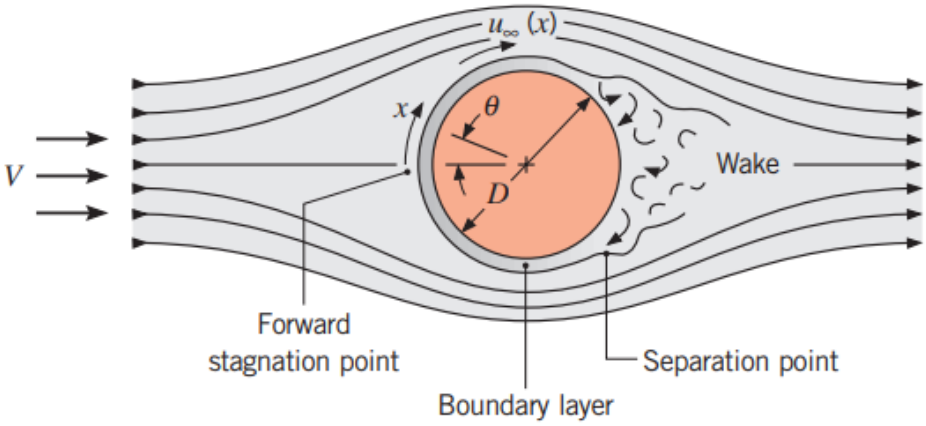

Figure 4: Cylinder in Cross Flow [9]

The heat transfer out of the cell is dependent on the temperature difference between the battery and the fluid, the area of the cell, and the total heat transfer coefficient. The heat transfer equation is shown shown in Equation 1.

$$\dot{Q} = hA\Delta T \tag{1}$$

The heat transfer coefficient is found using an empirical relationship for a cylinder in cross-flow discovered by Churchill and Bernstein [9] shown in Equation 2.

$$\bar{h} = \frac{k}{D}\left\{0.3 + \frac{0.62Re_D^{1/2}Pr^{1/3}}{\left[1+(0.4/Pr)^{2/3}\right]^{1/4}}\left[1+\left(\frac{Re_D}{282,000}\right)^{5/8}\right]^{4/5}\right\} \tag{2}$$

It should be noted that this relationship is developed for a cylinder with an infinite length which introduces error in the case of this finite length battery cell. The flow velocity is found by taking the volume flow rate of the pump and dividing it by the lateral cross-sectional area of the battery pack. This area spans the width of the vehicle at 1.5 m and has a height of the 18650 cells of 65 mm. After calculating the transient heat flow out of the battery, this heat flow is inputted into the thermal network which is discussed in section 3.4.

3.3 Wire Model

The heat generated in the electrical wire connecting the charging station to the battery pack is also modeled and simulated. The DC current runs from the charging station through one conductor into the battery pack and then back out of the battery pack through another conductor into the charging station to close the circuit. The total length of this circuit is assumed to be 10 m. The material of the wire is assumed to be copper, as copper is traditionally used for DC fast charge cables due to its high electrical conductivity. The radius of the copper conductor is 6.25 mm.

The electrical resistance per meter of copper wire (0.019 ohms mm^2/m) is a function of the temperature of the wire. As the temperature of the copper increases, the resistance increases so that a temperature factor of 0.000393 per $^\circ$ C is used to calculate the resistance of the wire as the wire temperature changes [10]. The heat transfer out of the wire occurs radially (see Figure 1) and follows the relationship described in Equation 1.

Notice that the heat generated in the wire is a function of the current flowing through the wire. Section 4.2 discusses this relationship further. The mass of the wire, along with the surface area of the wire is calculated and inserted into the thermal model shown in Figure 5.

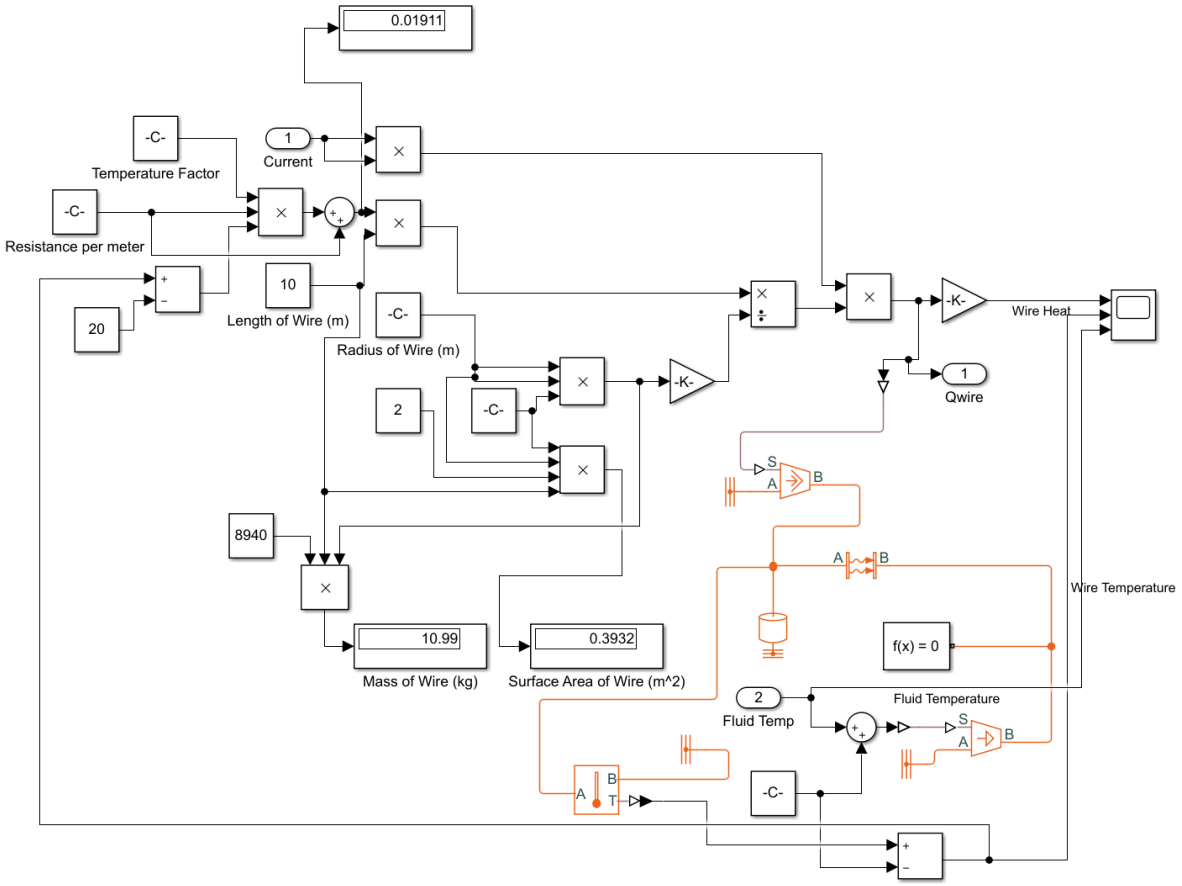

Figure 5: Simscape wire model

The fluid temperature calculated in section 3.4 is used to find the heat transfer rate out of the wire.

3.4 Thermal Network

The thermal network is comprised of a closed loop of coolant. A mixture of ethylene glycol and water is used to maintain compatibility with traditional automotive cooling systems. This thermal fluid recirculates between the vehicle and the battery pack to cool the battery pack during rapid charging. An ideal pump is used to pump the fluid at a constant rate of 200 liters/min. The flow rate is measured to calculate the velocity of the fluid as described in section 3.2. The fluid network is shown in Figure 6.

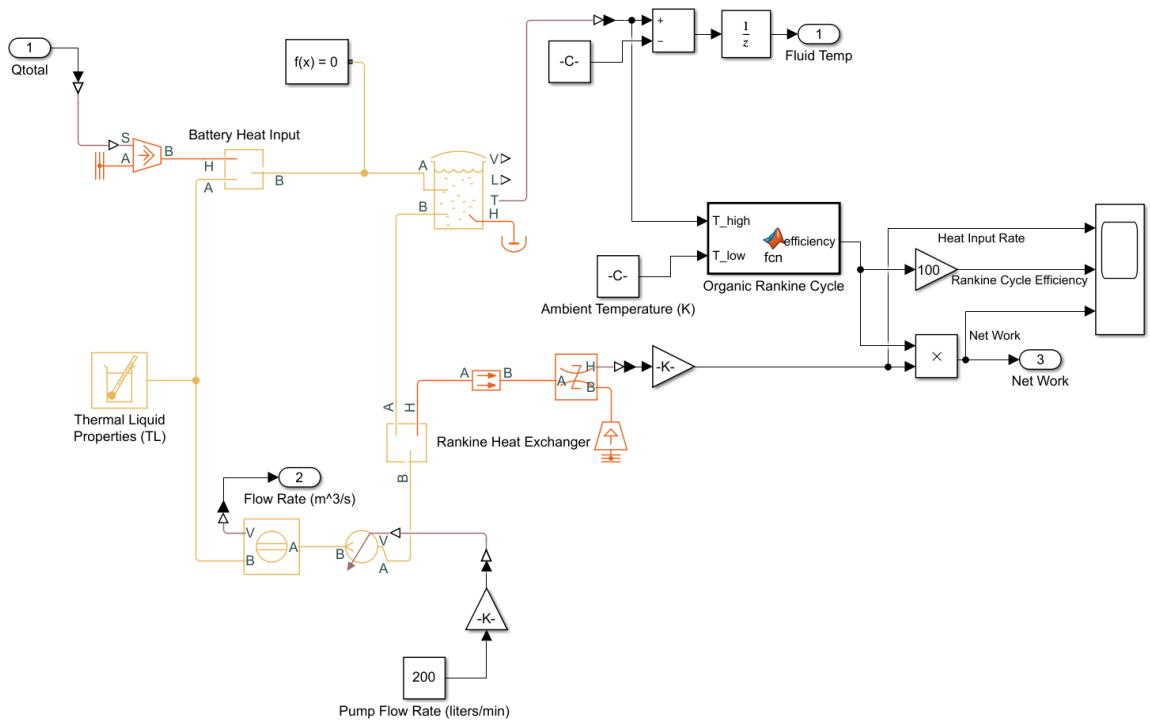

Figure 6: Simscape thermal-fluid model

The vehicle-level heat generation rate is used as the heat input of the thermal-fluid network. This heat generation rate is calculated by multiplying the cell heat generation rate derived in section 3.2 by the number of cells in the battery pack. The volume of fluid is defined to be 20 gallons and its temperature is measured using a temperature sensor attached to the fluid reservoir. The temperature of the fluid is also used to calculate the heat transfer rate of the cell described in section 3.2 and the wire described in section 3.3. Heat exits the fluid network through a heat exchanger with the organic Rankine cycle described in section 3.5.

The initial temperature of the fluid is set at 20° C. Using this model, there are two options for heat sinks; ambient atmospheric air and ambient geothermal average ground temperature. If the atmospheric temperature is above 13° C, the heat sink is set as the geothermal average ground temperature of 13° C. Conversely, if the atmospheric temperature is below 13° C, the heat sink is set as the atmospheric temperature. This method maximizes heat dissipation between the summer and winter.

3.5 Organic Rankine Cycle Model

The organic Rankine cycle is designed using a MATLAB script (See Appendix A for more information) that interpolates temperature-dependent specific entropy values from a REFPROP database. REFPROP is a tool created by the National Institute for Standards and Technologies (NIST) with highly accurate thermophysical data for a variety of different fluids [11]. Since the Rankine cycle is a two-phase cycle, the working fluid is selected from the REFPROP database to find an organic fluid that operates as both a liquid and a gas at moderate pressures at room temperature. R-134a is selected as the working fluid, as it is the most common working fluid that operates at a temperature range between 20 and 40° C. The temperature vs. specific entropy (T-S) diagram is created using the MATLAB script and plotted in Figure 7. Each line represents a different pressure. The lines left of the bell-shaped curve show fluid liquid states and the lines right of the bell-shaped curve show fluid vapor states.

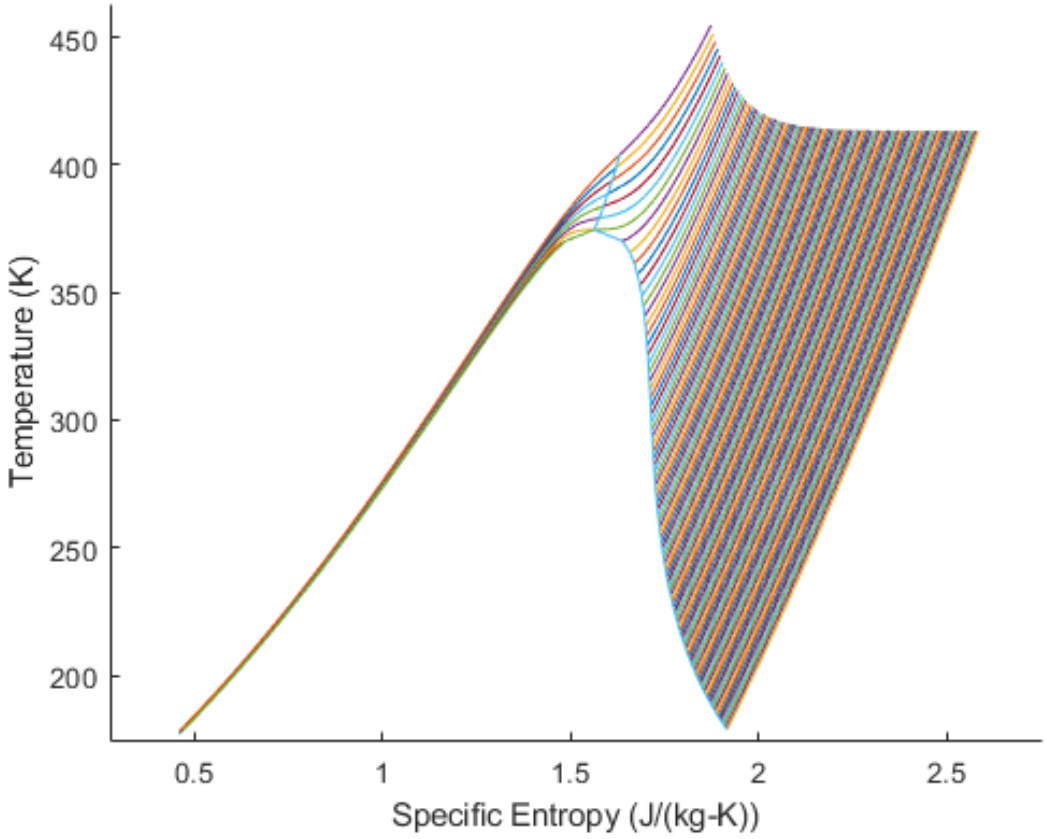

Figure 7: T-S diagram for R-134a (Data acquired from REFPROP)

State 1 is defined as the saturated liquid point at the lower temperature boundary. The MATLAB script receives a low temperature input and uses Figure 7 to interpolate the specific entropy and pressure values. State 4 is calculated in a similar manner at the saturated vapor point. State 3 is calculated at the same specific entropy as state 3 but the pressure is increased until the temperature of the vapor reaches the thermal-fluid temperature described in section 3.4. State 2 is calculated at the same pressure as State 3 and the same specific entropy as State 1. With the temperature, pressure, and specific entropy known at all 4 states, the relevant work flows and heat flows are calculated. The efficiency of a Rankine cycle is defined by Equation 3.

$$\eta = \frac{\dot{Q}_{in}}{\dot{W}_{turbine} - \dot{W}_{pump}} \tag{3}$$

The power generated by the Rankine cycle is computed by multiplying the heat in times the efficiency of the cycle. Throughout the simulation, this efficiency is calculated at each time step as the fluid temperature fluctuates. The charging rate input described in section 3.6 is subtracted by the power generated by the Rankine cycle to find the actual charging rate.

3.6 Top-Level System Model

The top-level system model (shown in Figure 8) integrates the battery cell model, wire model, thermal network, and organic Rankine cycle model into 1 system. At this level, the overall vehicle voltage architecture is defined to be either 400 V or 800 V. The number of batteries is set so that the total battery capacity is 100 kWh. The charge current is set to a rate of 15C and the battery cross-sectional area is defined to span the entire width of the vehicle with a height of 65 mm (the height of an 18650 cell).

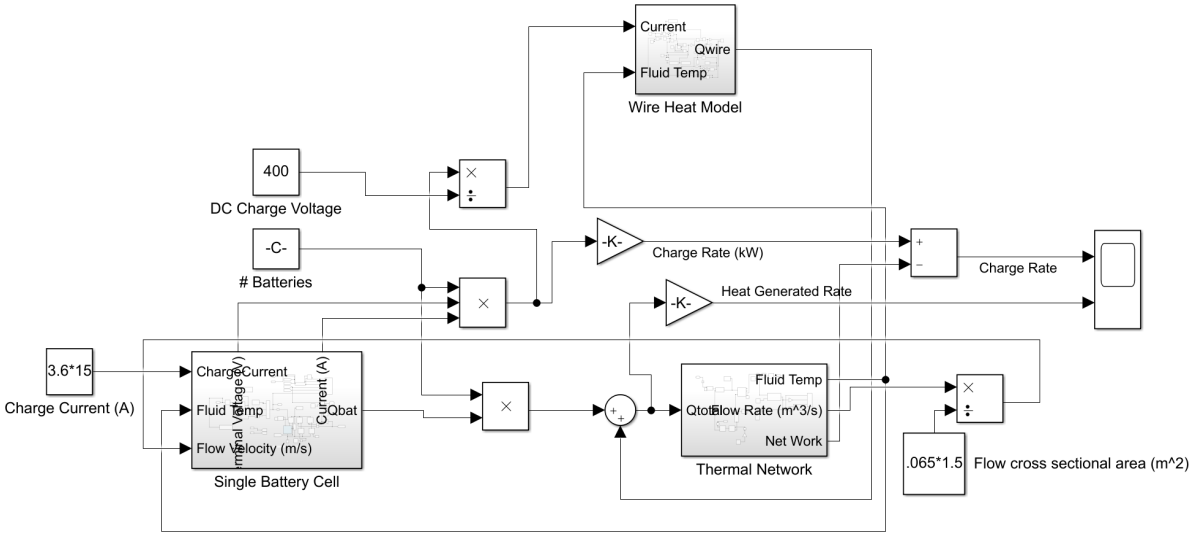

Figure 8: Simscape vehicle-level model

The fluid temperature and flow velocity from the thermal-fluid network is used to calculate the heat transfer rate out of the battery cell. This rate is multiplied by the number of cells in the pack and used as the heat input for the thermal-fluid network. The vehicle charge rate is calculated by multiplying the cell voltage, cell current, and cell

number. The resulting charge rate is divided by the charger voltage to find the current that travels through the charging cable. This current is inserted into the wire model. The heat generated in the wire model is added to the heat generated by the battery pack to find the total heat rate entering the thermal fluid network. The power that the Rankine cycle generates is subtracted from the nominal charge rate to find the actual charge rate.

The simulation is set to stop when the cell SOC reaches 1, indicating that the battery pack is fully charged. The following variables are plotted using the scope for further analysis in section 4; cell charge rate, cell charging current, cell terminal voltage, cell SOC, cell temperature, cell heat generation rate, wire heat generation rate, wire temperature, fluid temperature, Rankine cycle heat input, Rankine cycle efficiency, Rankine cycle net work, vehicle charge rate, and vehicle heat generation rate.

4 Results

The results section is divided between 4 experiments. The first experiment utilizes a 400 V architecture with an ambient outside temperature of 20° C. The second experiment utilizes a 800 V architecture with an ambient outside temperature of 20° C. The third experiment utilizes a 400 V architecture with a higher (summer) ambient outside temperature of 37° C. The fourth experiment utilizes a 400 V architecture with a lower (winter) ambient outside temperature of 0° C. These experiments are chosen to show the advantages and disadvantages of two voltage architectures as well as the performance of the cooling system across a range of real-world ambient temperature conditions.

4.1 400 V Architecture Results

The results for the 400 V architecture are shown below. This experiment is used as the baseline for the subsequent experiments.

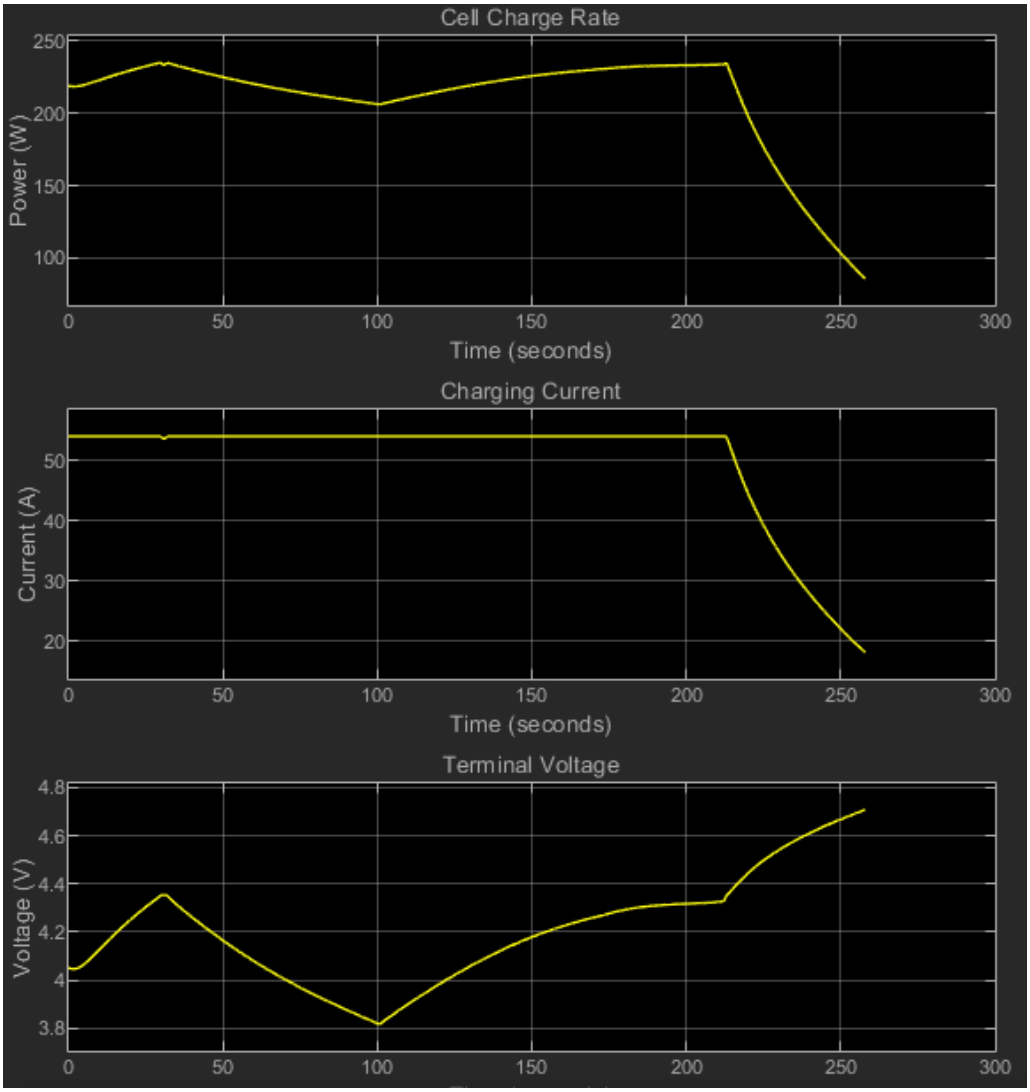

Figure 9: Cell level charge data using a 400V architecture

Figure 9 shows a standard CCCV charging scheme. The current is at its maximum until the terminal voltage reaches 4.35 V. At this point, the current decreases to reduce heat generation at the end of the charge cycle. Note that the sharp discontinuities found in this figure, as well as the rest of the figures is due to insufficient Look-up-table (LUT) data acquired from T. Huria et al. [5]. This empirically generated LUT data is used to correlate resistance and capacitance at various cell temperatures and SOCs.

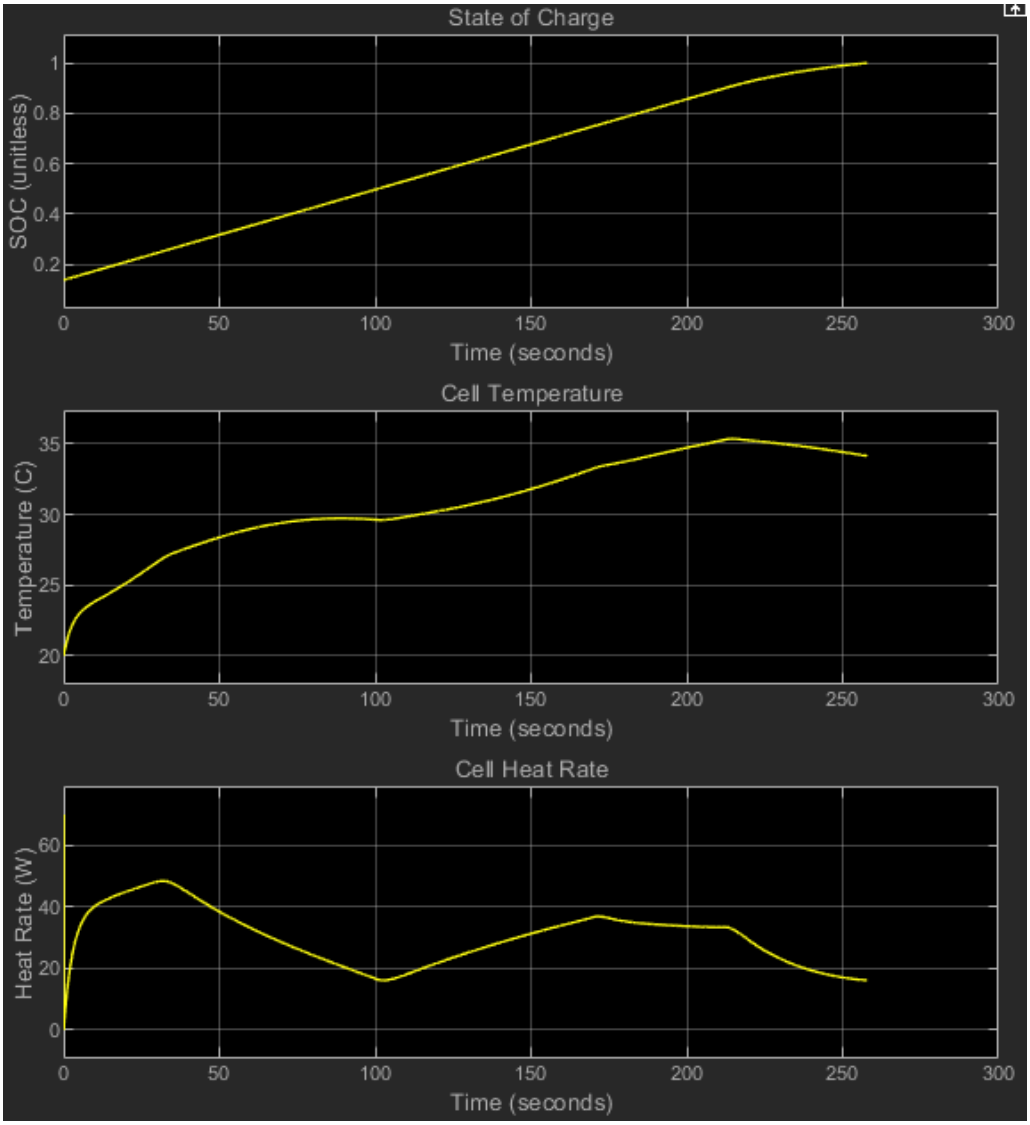

Figure 10: Cell level temperature and heat rate data using a 400V architecture

Figure 10 shows that even though current is reduced at the end of the charge cycle, heat generation stays relatively constant. This is due to the temperature dependent resistance of the cell. As the temperature of the cell increases, the resistance also increases. The peak cell temperature is just above 35° C which occurs toward the end of the charging cycle.

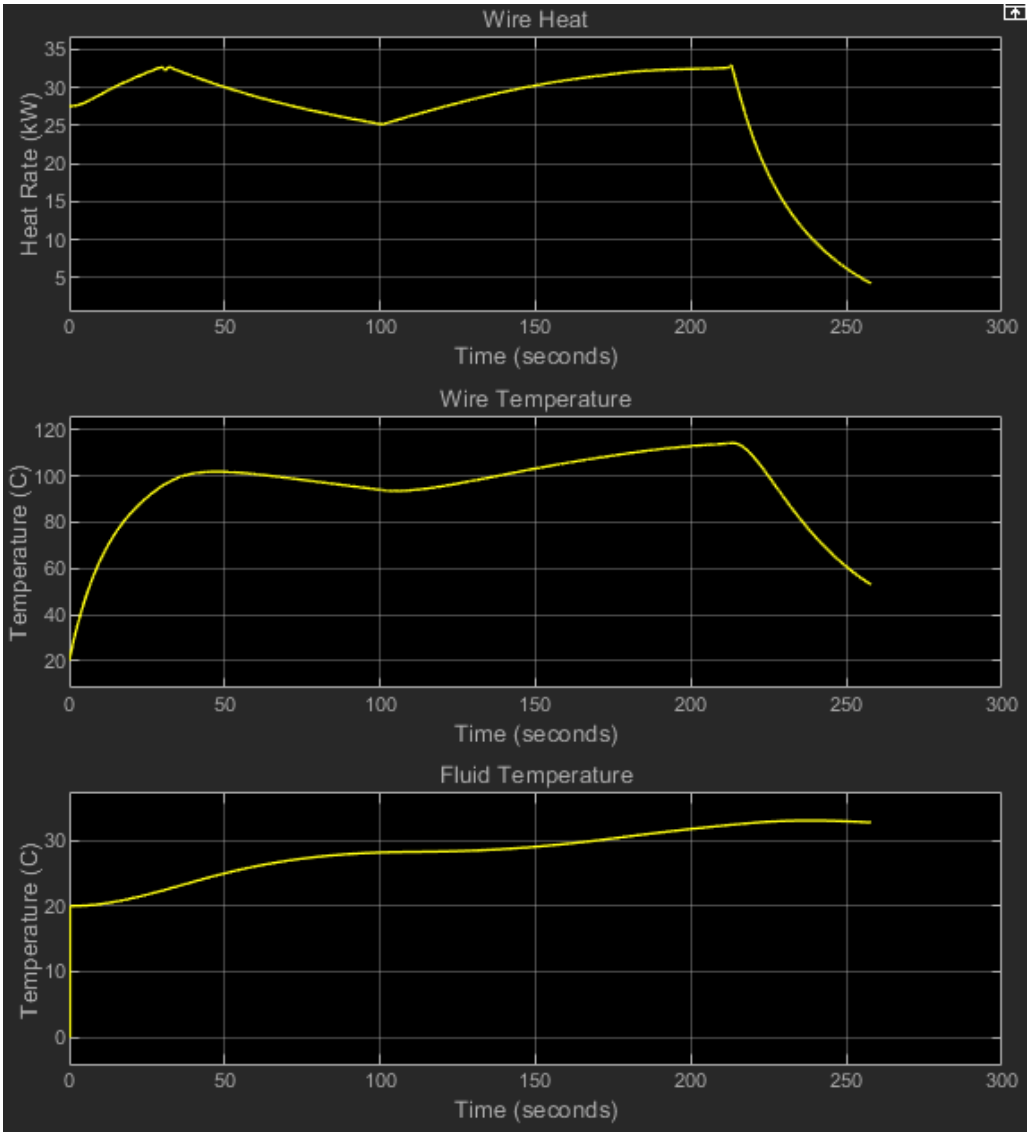

Figure 11: Wire temperature and heat rate data using a 400V architecture

Figure 11 shows that the heat generated by the wire is also maximized near the end of the charging cycle. Since the wire resistance is dependent on the voltage architecture. The temperature of the copper conductor using a 400 V architecture is high at close to 120° C. The fluid temperature increases throughout the charging cycle as it absorbs the heat generated by the battery cell and the wire. This heat is dissipated through the Rankine cycle at a lower rate than the the heat absorption rate.

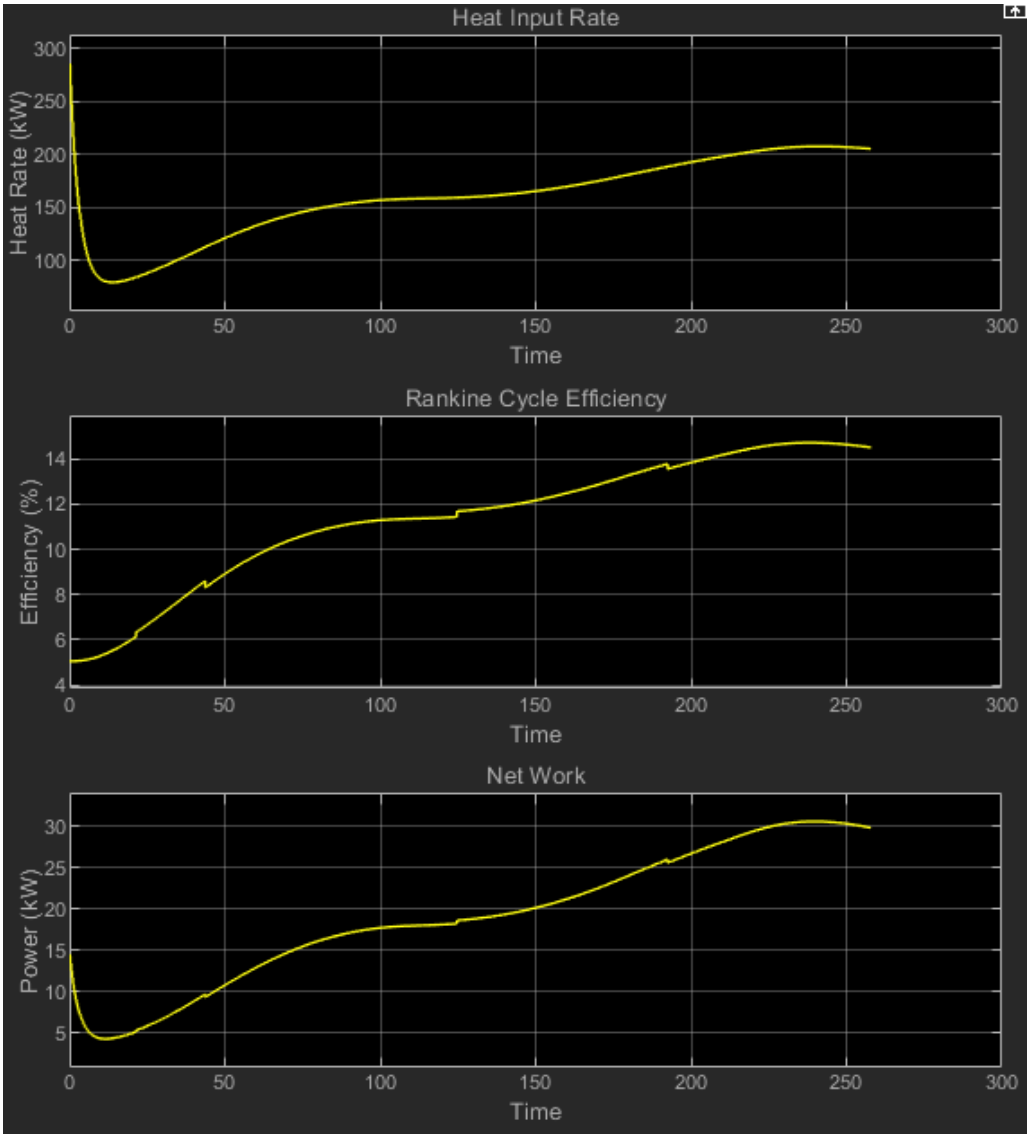

Figure 12: Organic Rankine cycle efficiency and work using a 400V architecture

Figure 12 shows that the Rankine cycle efficiency increases as the fluid temperature increases. Since the heat sink temperature is constant, the increase in fluid temperature leads to a larger temperature difference, increasing the efficiency of the Rankine cycle. Note that there is a discontinuity in the solver at the beginning of the simulation which creates a spike in the heat rate. The other experiments also exhibit this issue and initial time response data should be ignored for the purposes of this analysis.

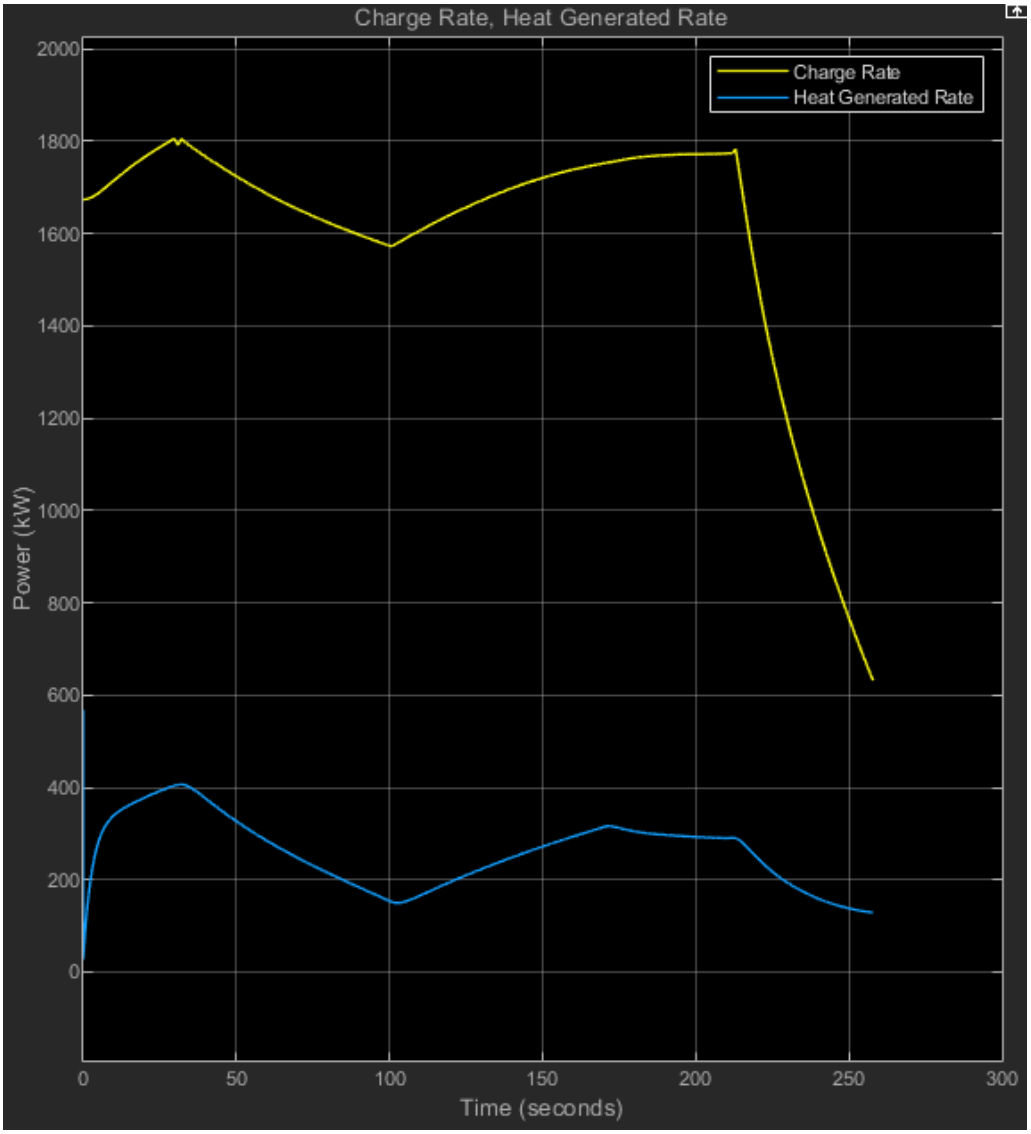

Figure 13: Vehicle level charge rate and heat rate results using a 400V architecture

Figure 13 shows the overall charge rate achieved and subsequent heat generated by the battery cell and the wire. The peak charge rate is relatively constant around 1700 kW until the current is reduced near the end of the charge cycle. The heat generation rate is relatively constant throughout the charge cycle with an average just over 200 kW. The 0-100% charge time is just over under 260 seconds.

4.2 800 V Architecture Results

The results for the 800 V architecture are shown below.

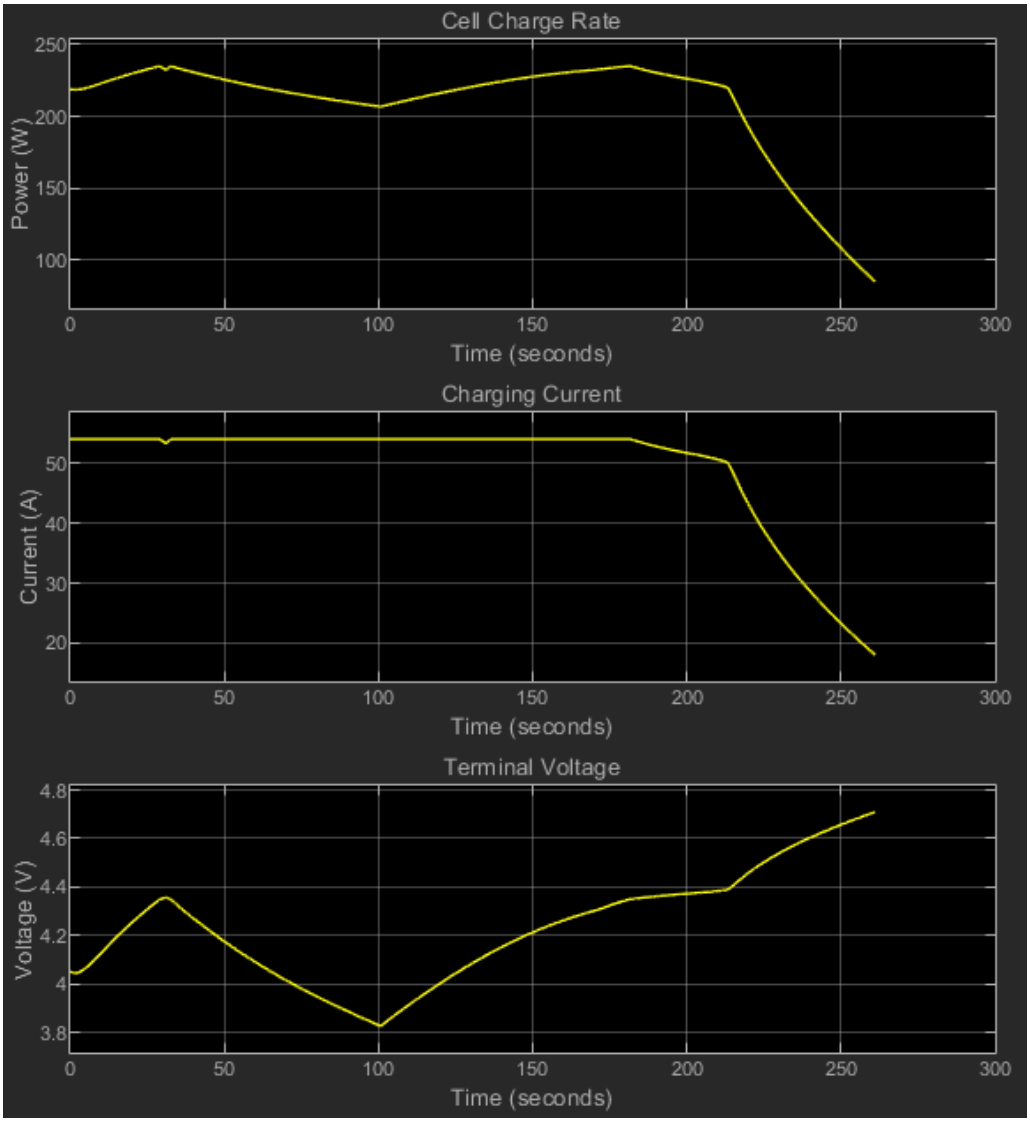

Figure 14: Cell level charge data using a 800V architecture

Figure 14 shows that the charge current is reduced about 40 seconds sooner than in the 400 V case. The terminal voltage decreases as the temperature of the battery increases. With an 800 V architecture, the battery temperature is lower which increases the terminal voltage thus causing the current to be reduced earlier.

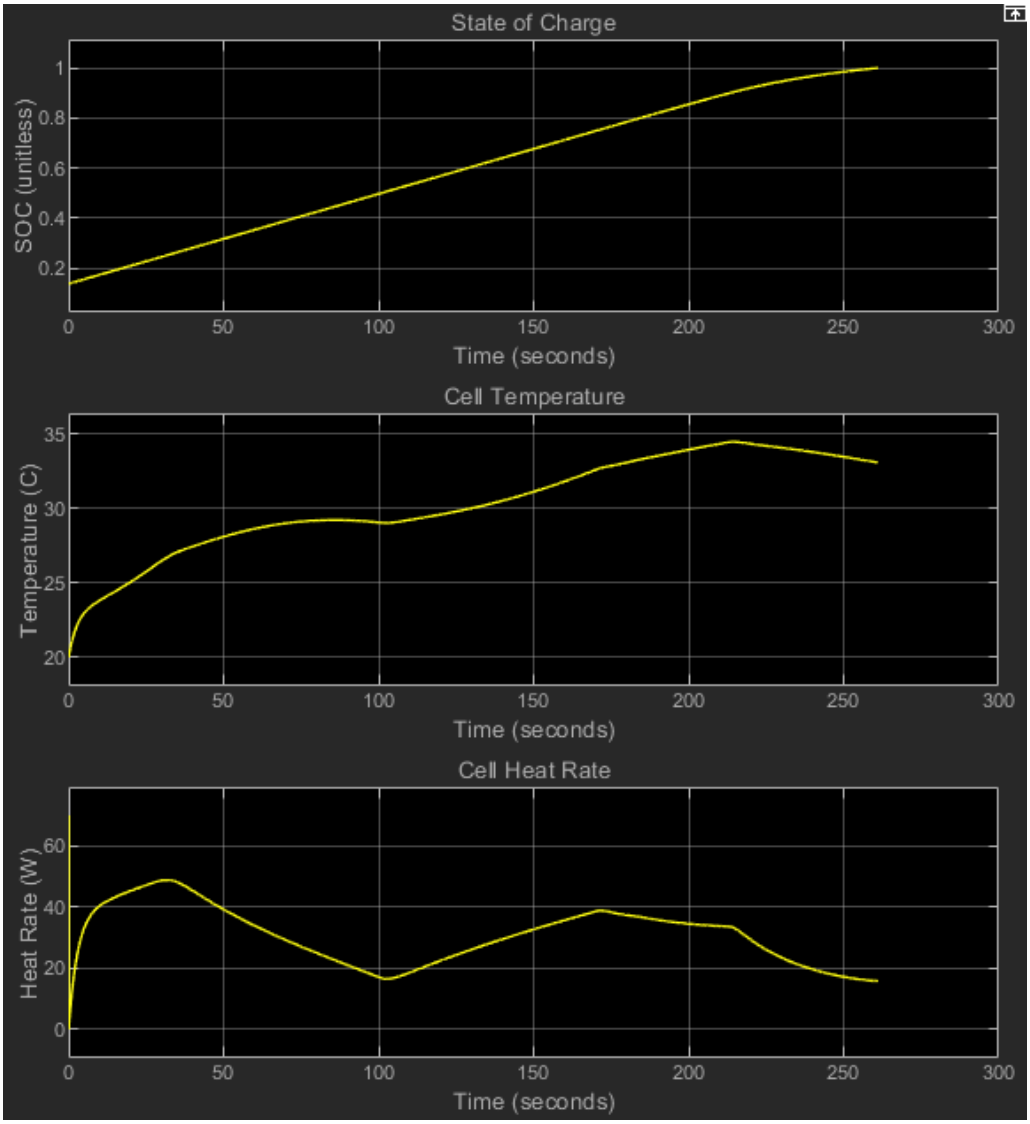

Figure 15: Cell level temperature and heat rate data using a 800V architecture

When compared to Figure 10, Figure 15 exhibits a similar trend. The cell temperature is slightly lower due to the lower system fluid temperature.

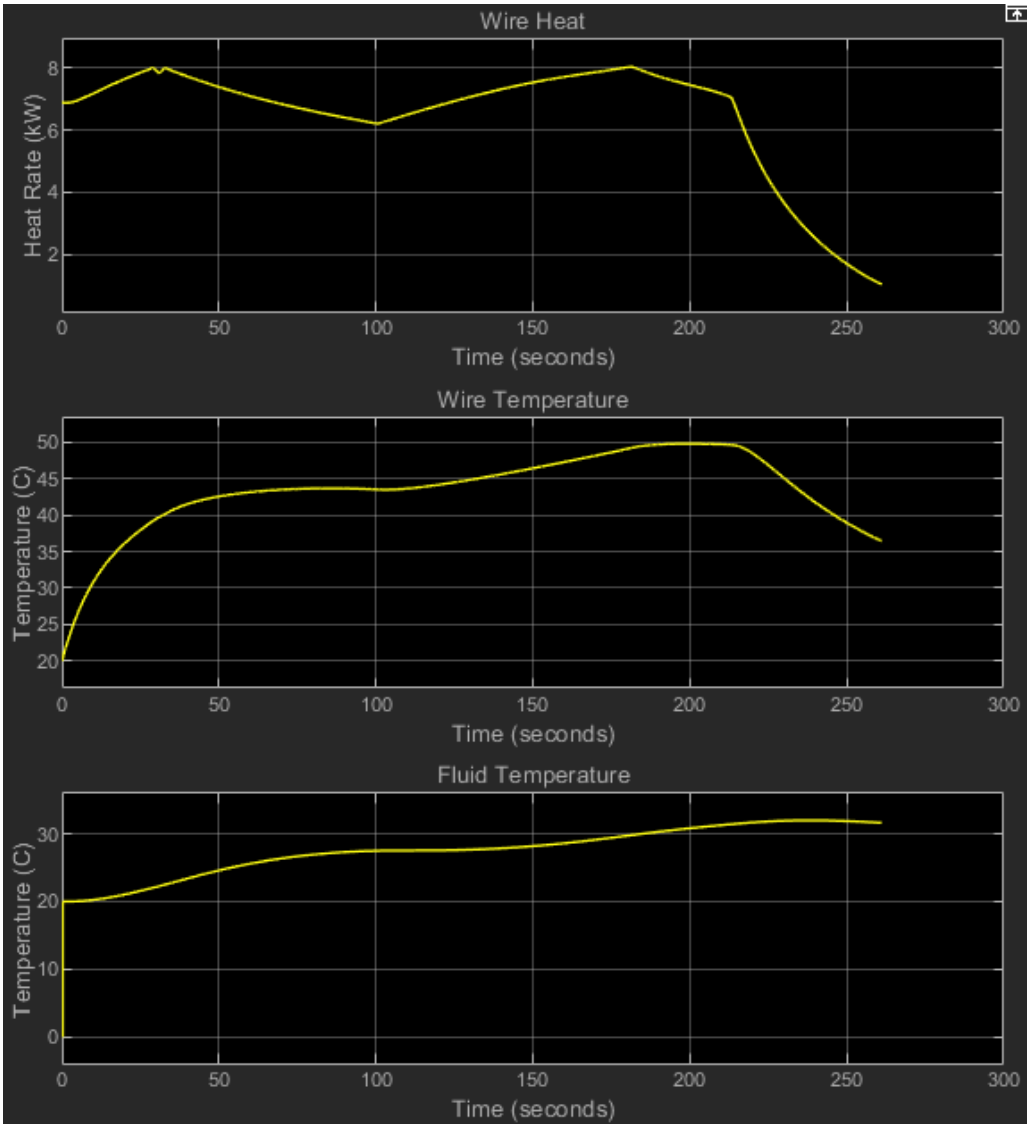

Figure 16: Wire temperature and heat rate data using a 800V architecture

Figure 16 shows a heat generation rate in the wire that is much lower than the heat generated rate in Figure 11. The peak wire heat generation rate is 8 kW compared to 33 kW from the 400 V experiment. This large reduction in heat translates into a peak wire temperature of 50° C, compared to a peak wire temperature of just under 120° C in the 400 V experiment. The fluid temperature maximum is also reduced to 32° C, compared to 33° C from the 400 V experiment.

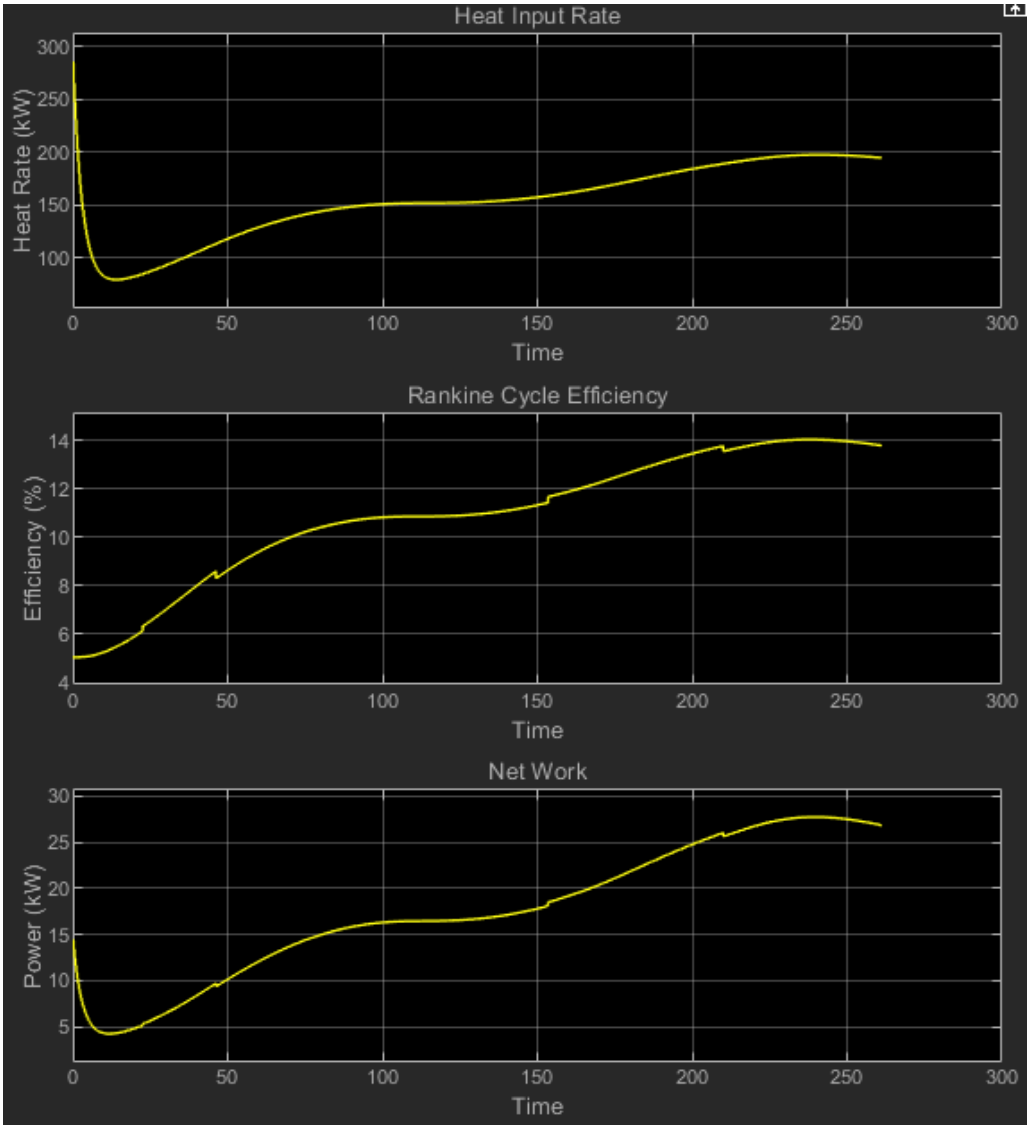

Figure 17: Organic Rankine cycle efficiency and work using a 800V architecture

Figure 17 shows a reduction in the fluid temperature relates to a reduction in the Rankine cycle efficiency. The efficiency decreases by 1% compared to a 400 V architecture.

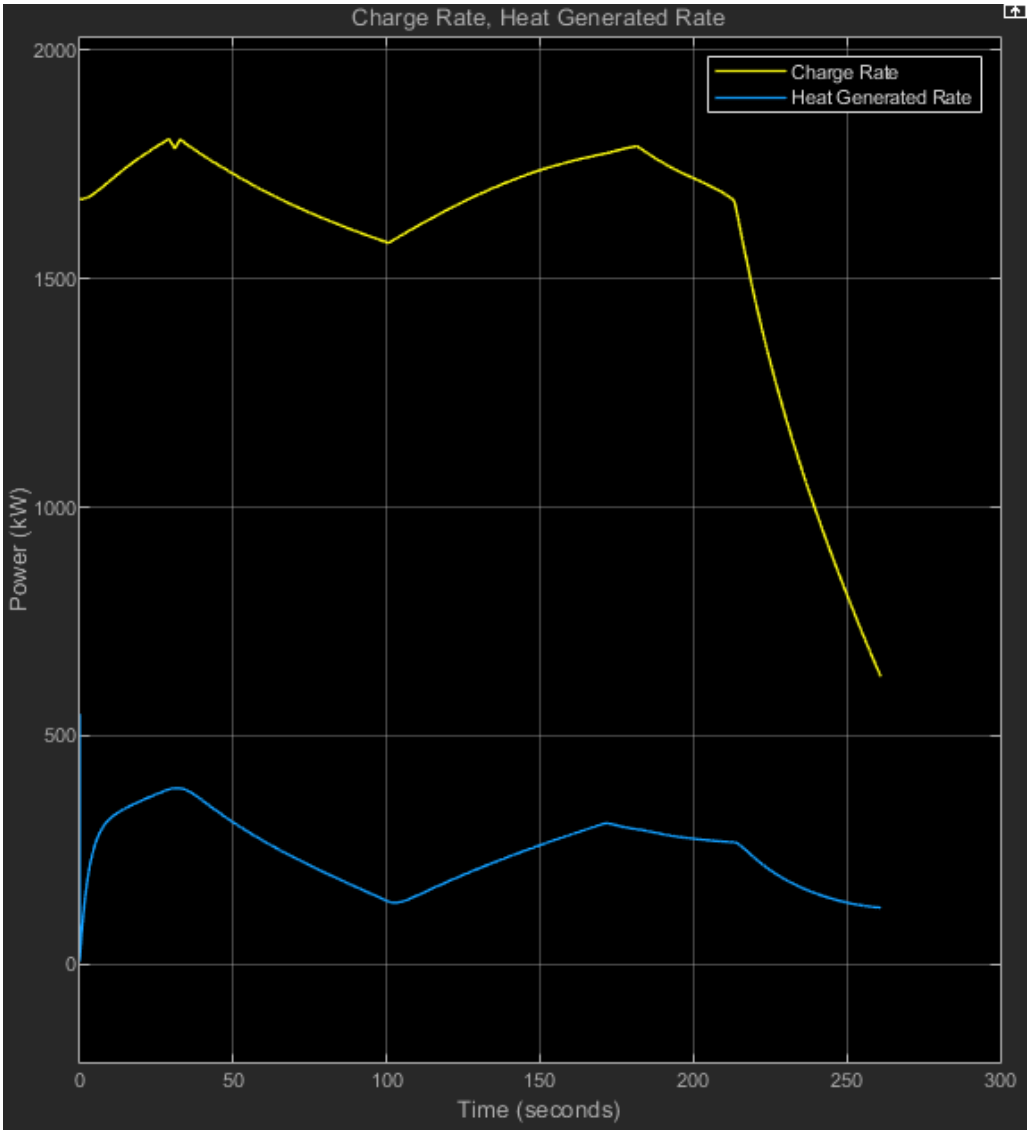

Figure 18: Vehicle level charge rate and heat rate results using a 800V architecture

Figure 18 shows that the overall charge rate is similar to the charge rate shown in Figure 13. Since the current is reduced sooner, however, the charge takes about 5 seconds longer to complete. The heat generation rate is reduced by about 20 kW throughout the charge cycle due the the decrease in current flowing through the charge cable.

4.3 High Ambient Temperature Results

The results below use an ambient outside temperature of 37° C and a 400 V architecture. A geothermal heat sink with a temperature of 13° C is used in this configuration.

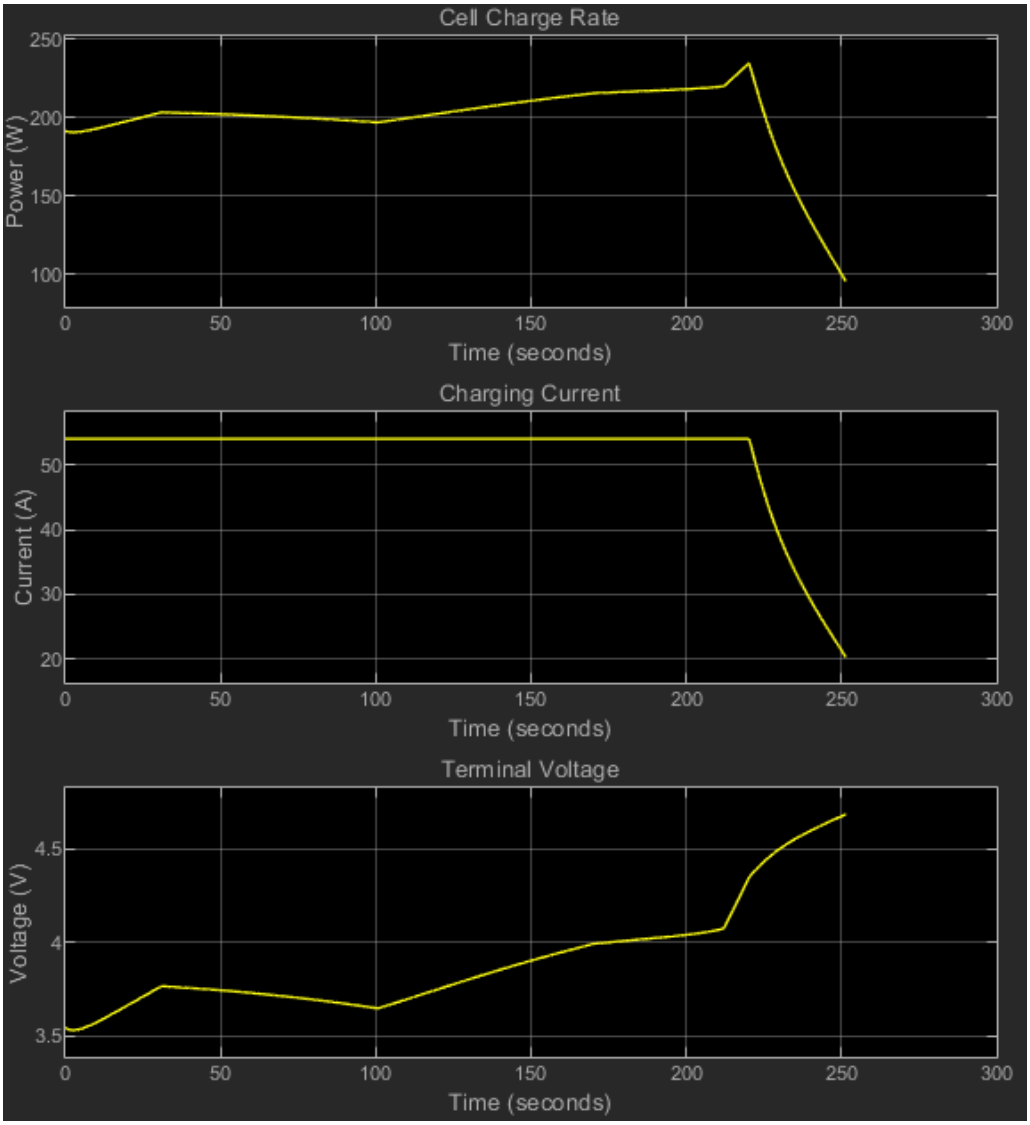

Figure 19: Cell level charge data using a 400V architecture at an outside temperature of 100 Fahrenheit

Compared to Figure 9, Figure 19 shows that the elevated ambient temperature allows the cells to charge at the maximum current rate for longer, as the terminal voltage stays below 4.35 V for longer. This shortens the charge time by about 5 seconds, compared to the 20° C ambient temperature case.

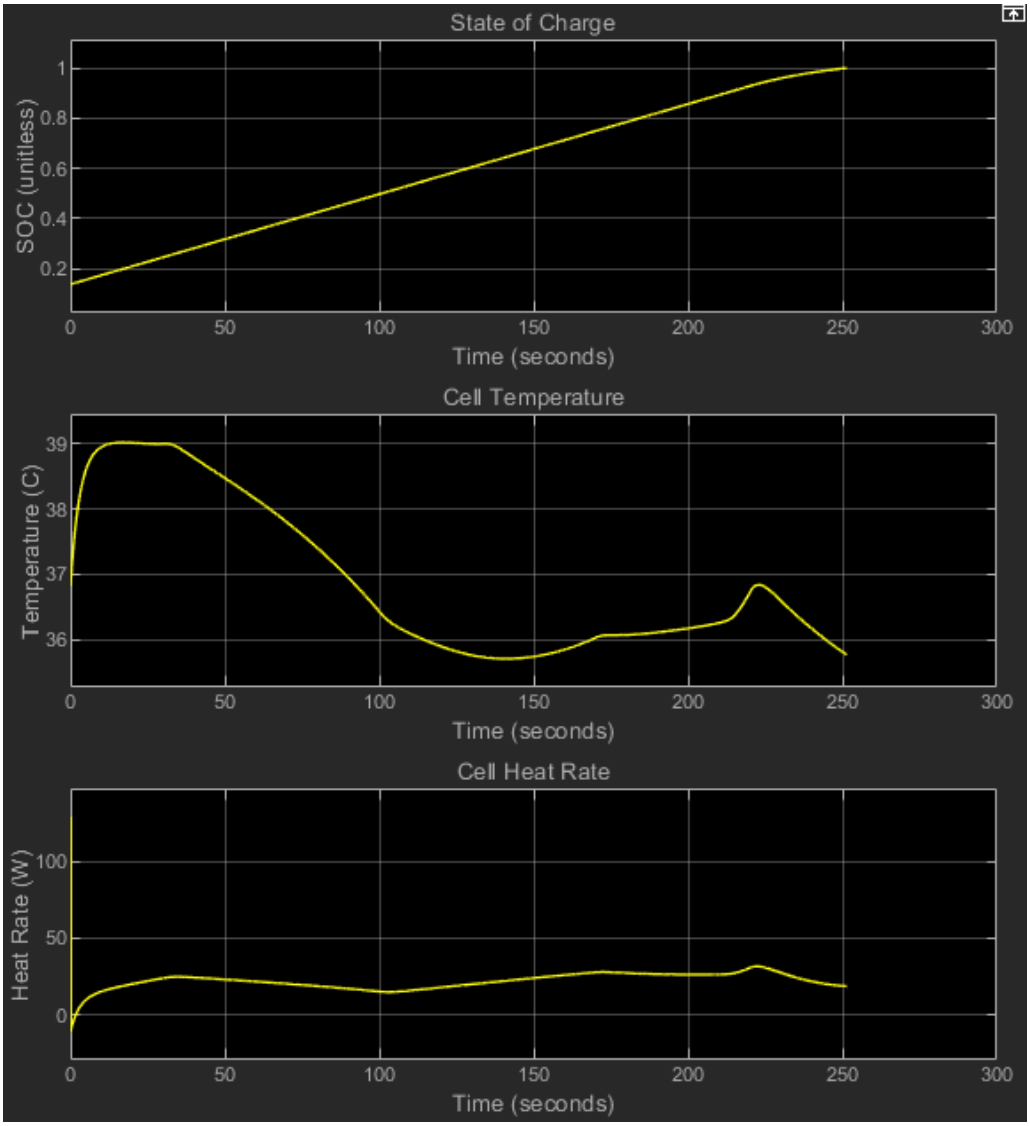

Figure 20: Cell level temperature and heat rate data using a 400V architecture at an outside temperature of 100 Fahrenheit

Figure 20 shows that the maximum cell temperature is reached early in the charge cycle at around 10 seconds. This cell temperature stays below 40° C (the threshold at which battery degradation begins to occur) and decreases throughout most of the charge cycle.

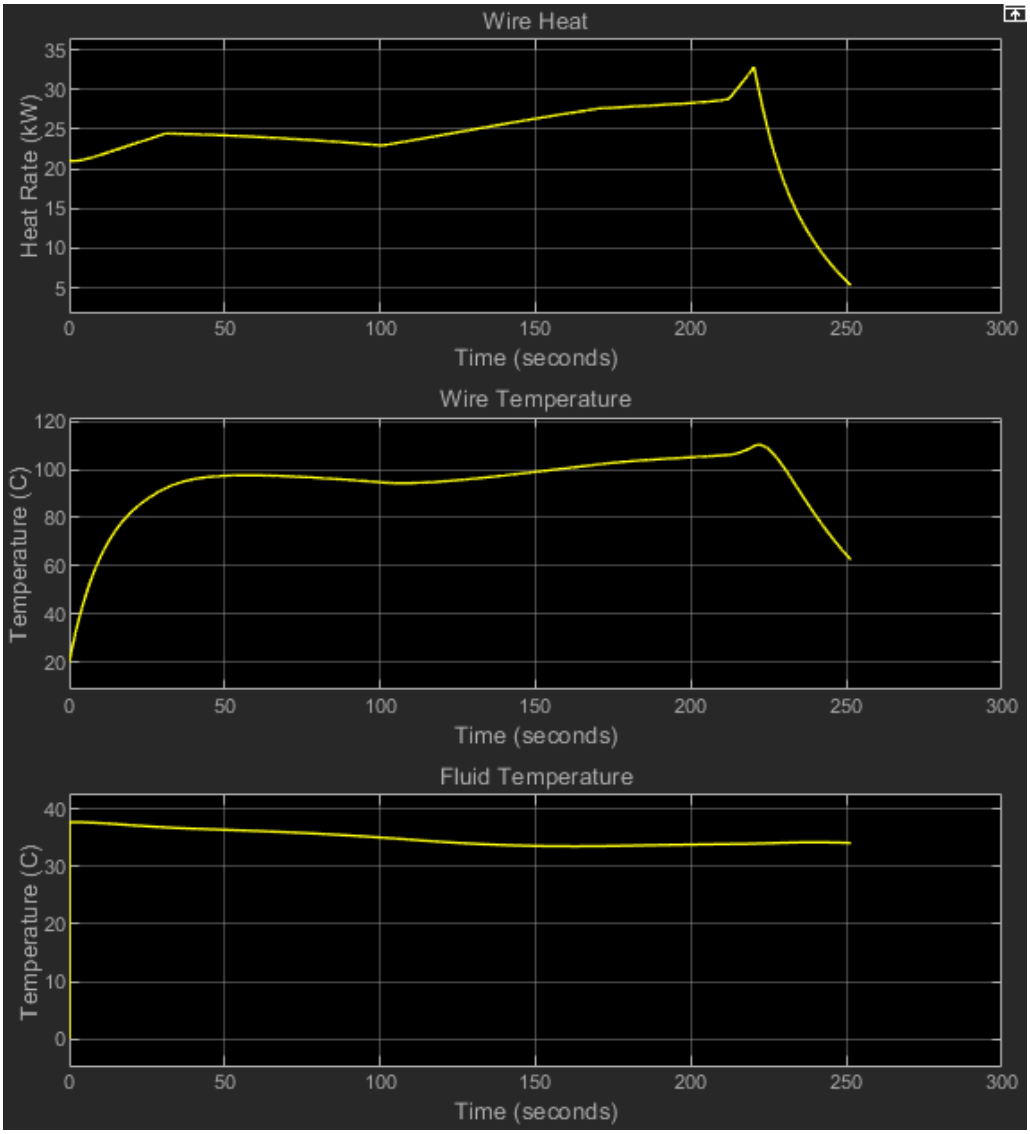

Figure 21: Wire temperature and heat rate data using a 400V architecture at an outside temperature of 100 Fahrenheit

Similarly, Figure 21 shows that the temperature of the fluid decreases slightly throughout the charge cycle. This is in contrast with the case shown in Figure 11. The fluid temperature decreases as the heat dissipation rate is greater in this case due to the larger temperature difference between the battery cell and the ground temperature. The wire temperature and heat generation rate is similar to the baseline case.

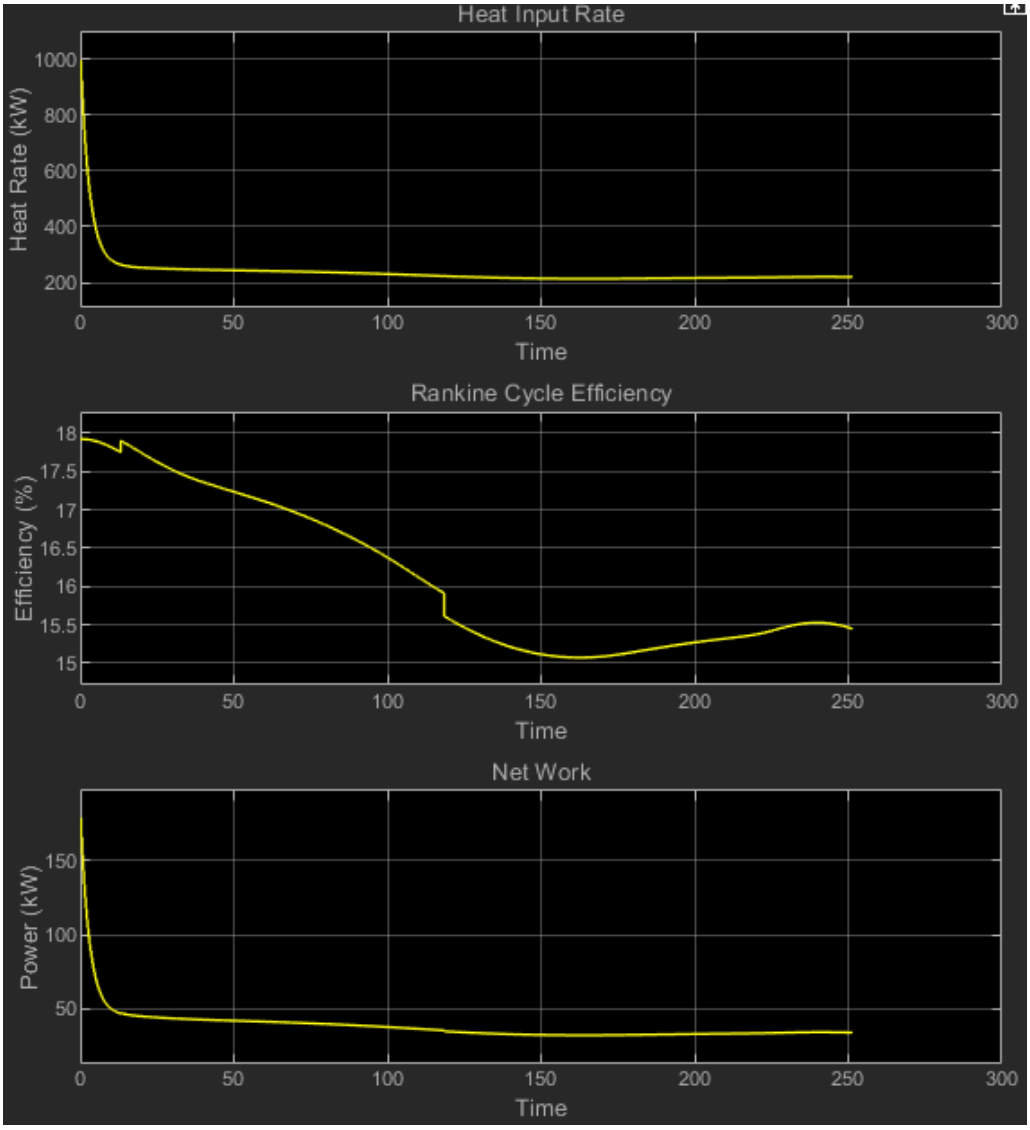

Figure 22: Organic Rankine cycle efficiency and work using a 400V architecture at an outside temperature of 100 Fahrenheit

Figure 22 shows that the Rankine cycle efficiency peaks in the beginning of the charge cycle due to the high initial fluid temperature. The peak Rankine cycle efficiency is 18% which is higher than the baseline efficiency of 15% shown in Figure 12. Furthermore, the maximum power generated by the Rankine cycle is about 50 kW in this case, versus about 30 kW in the baseline case.

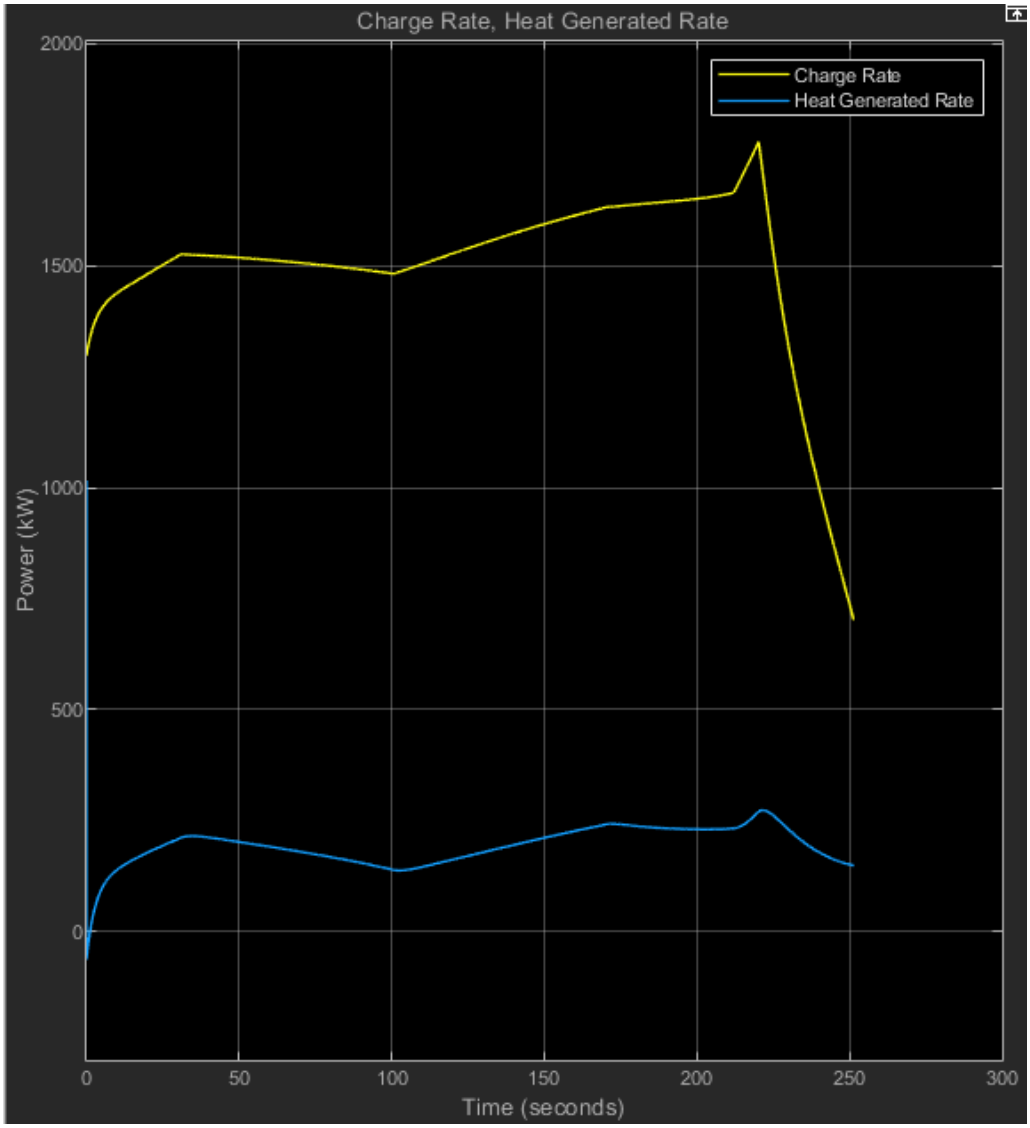

Figure 23: Vehicle level charge rate and heat rate results using a 400V architecture at an outside temperature of 100 Fahrenheit

Figure 23 shows that the average charge rate is about 1600 kW compared to the baseline case of 1700 kW. The heat generation rate is similar to the baseline case. The charge time is reduced by about 5 seconds to 250 seconds, compared to the baseline case shown in Figure 13.

4.4 Low Ambient Temperature Results

The results below use an ambient outside temperature of 0° C and a 400 V architecture. The atmosphere is used as the heat sink with a temperature of 0° C in this

configuration.

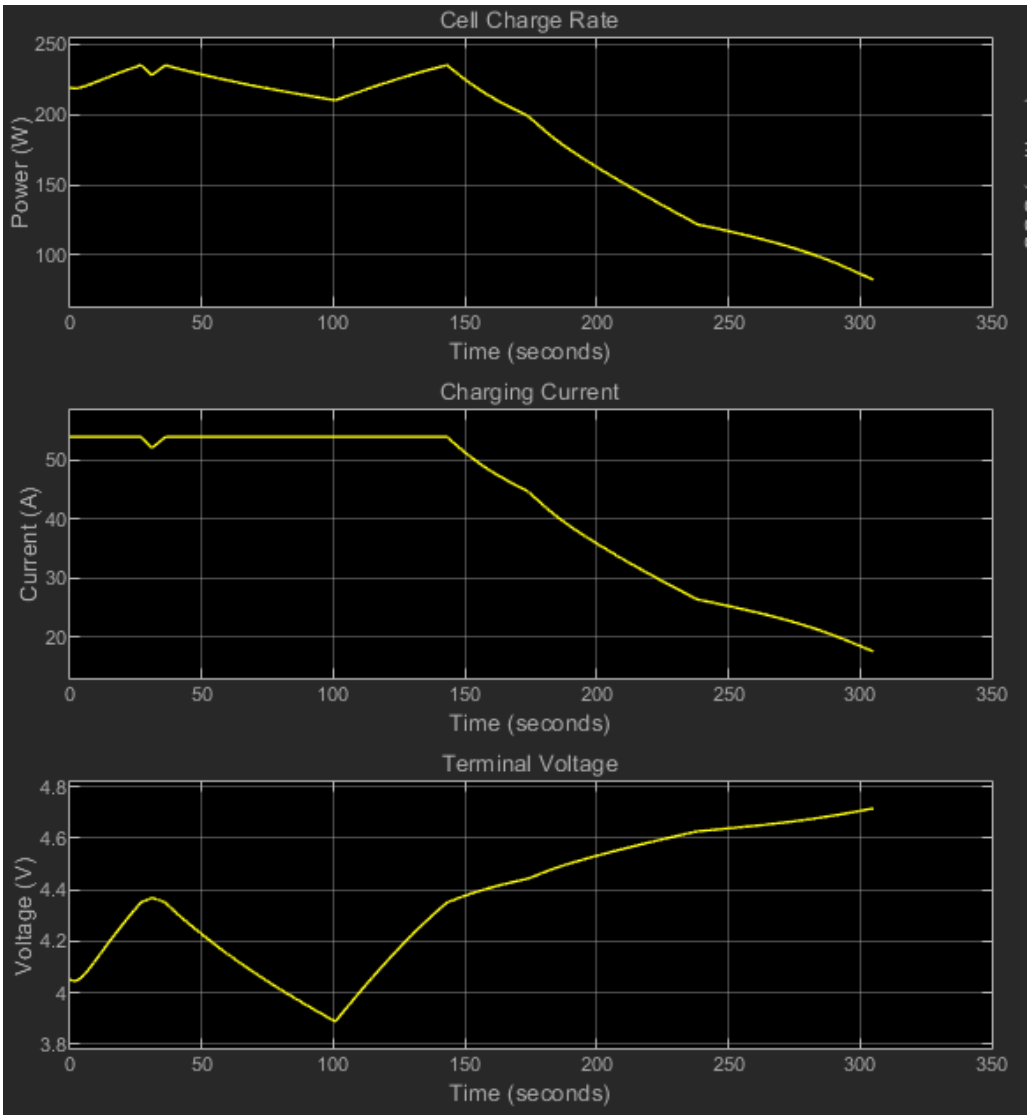

Figure 24: Cell level charge data using a 400V architecture at an outside temperature of 32 Fahrenheit

Figure 24 shows that the cell reaches a terminal voltage of 4.35 V early on in the charge cycle. This reduces the charge current but as the cell continues to heat up, the terminal voltage decreases and the charge rate returns to its maximum until 145 seconds at which point it begins to decrease. This takes place about 70 seconds earlier than the baseline case shown in Figure 9.

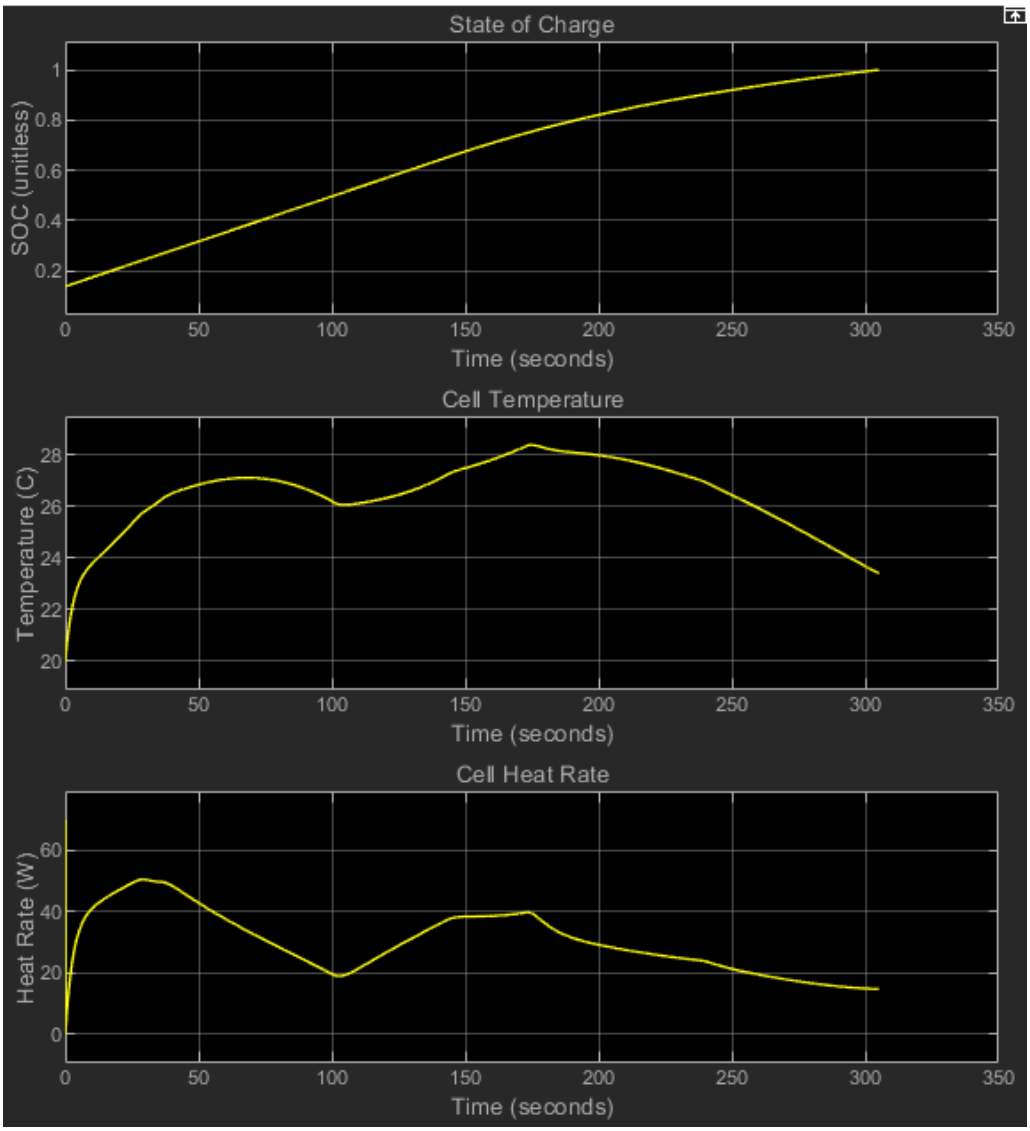

Figure 25: Cell level temperature and heat rate data using a 400V architecture at an outside temperature of 32 Fahrenheit

Figure 25 shows that the cell reaches its maximum temperature of around 28° C about halfway through the charge cycle. Due the the reduction in current earlier in the charging cycle, the SOC is more parabolic compared to cases with higher ambient temperatures.

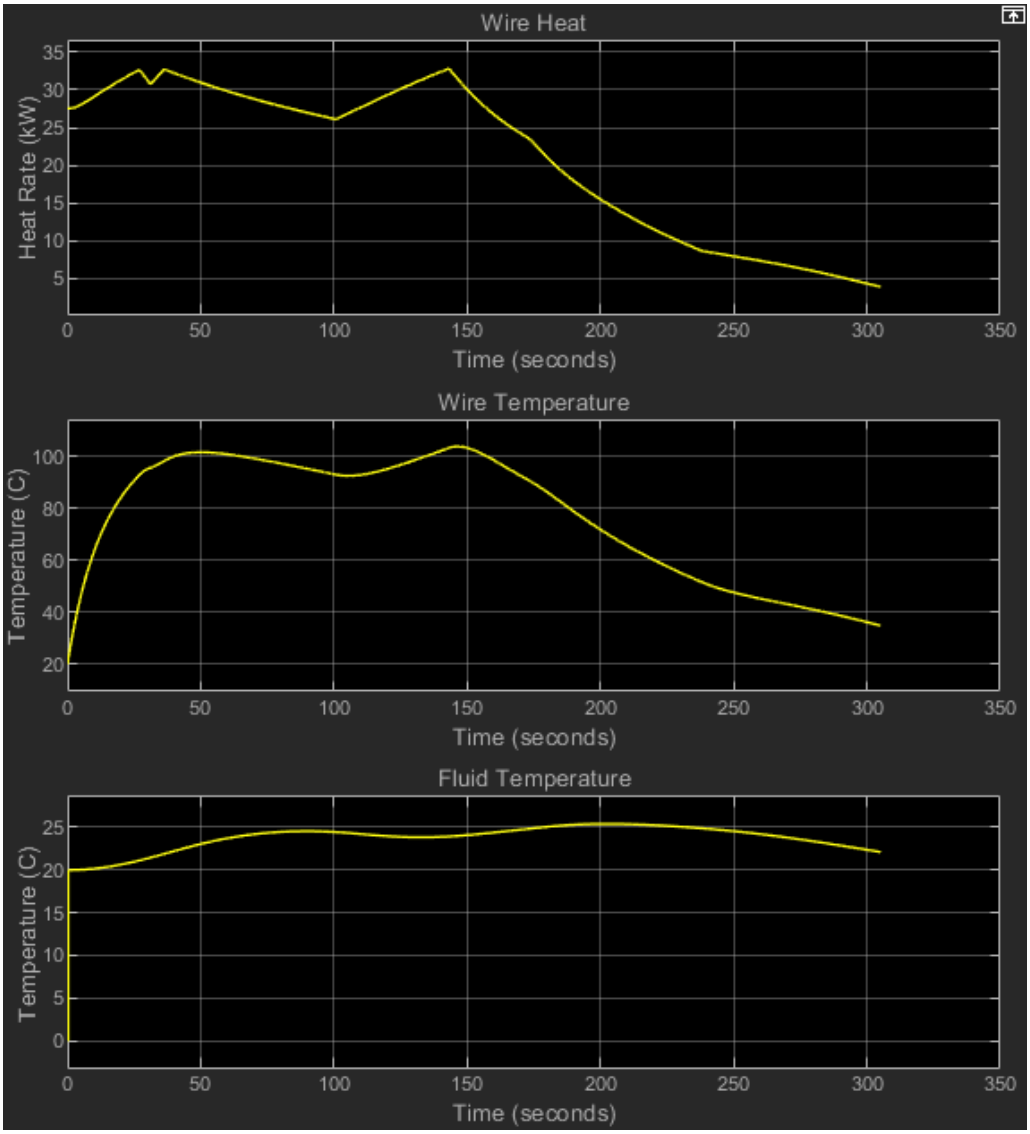

Figure 26: Wire temperature and heat rate data using a 400V architecture at an outside temperature of 32 Fahrenheit

Figure 26 shows that the wire temperature is reduced by about 10° C versus the baseline case shown in Figure 11. The fluid temperature stays relatively constant at around 25° C throughout the charge cycle, compared to the steady increase shown in the baseline.

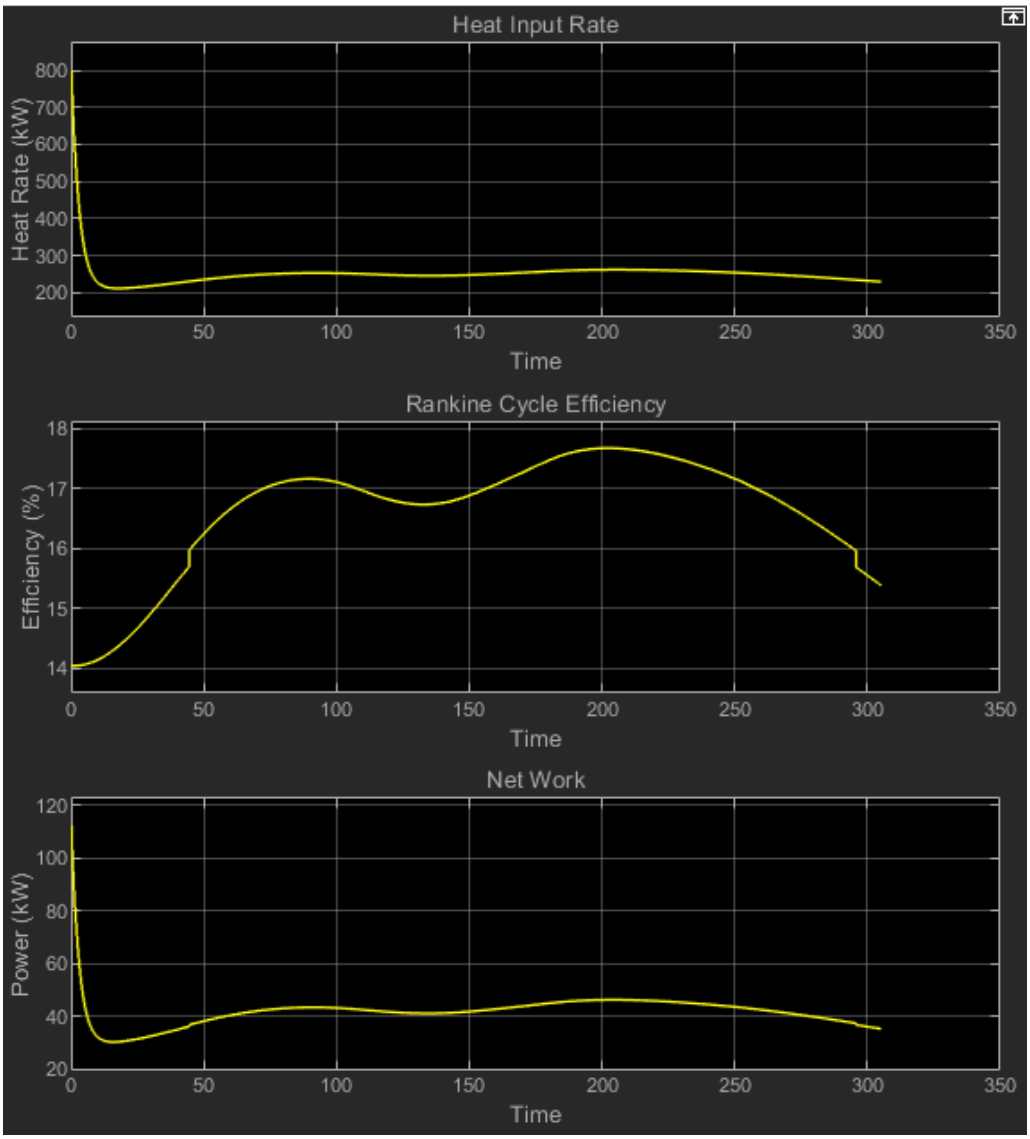

Figure 27: Organic Rankine cycle efficiency and work using a 400V architecture at an outside temperature of 32 Fahrenheit

Figure 27 shows a Rankine cycle peak efficiency just below 18% which is higher than the efficiency of 15% shown in Figure 12 even though the fluid temperature is lower throughout the charge cycle. The average Rankine cycle power is also higher, at 40 kW versus 20 kW from the baseline case.

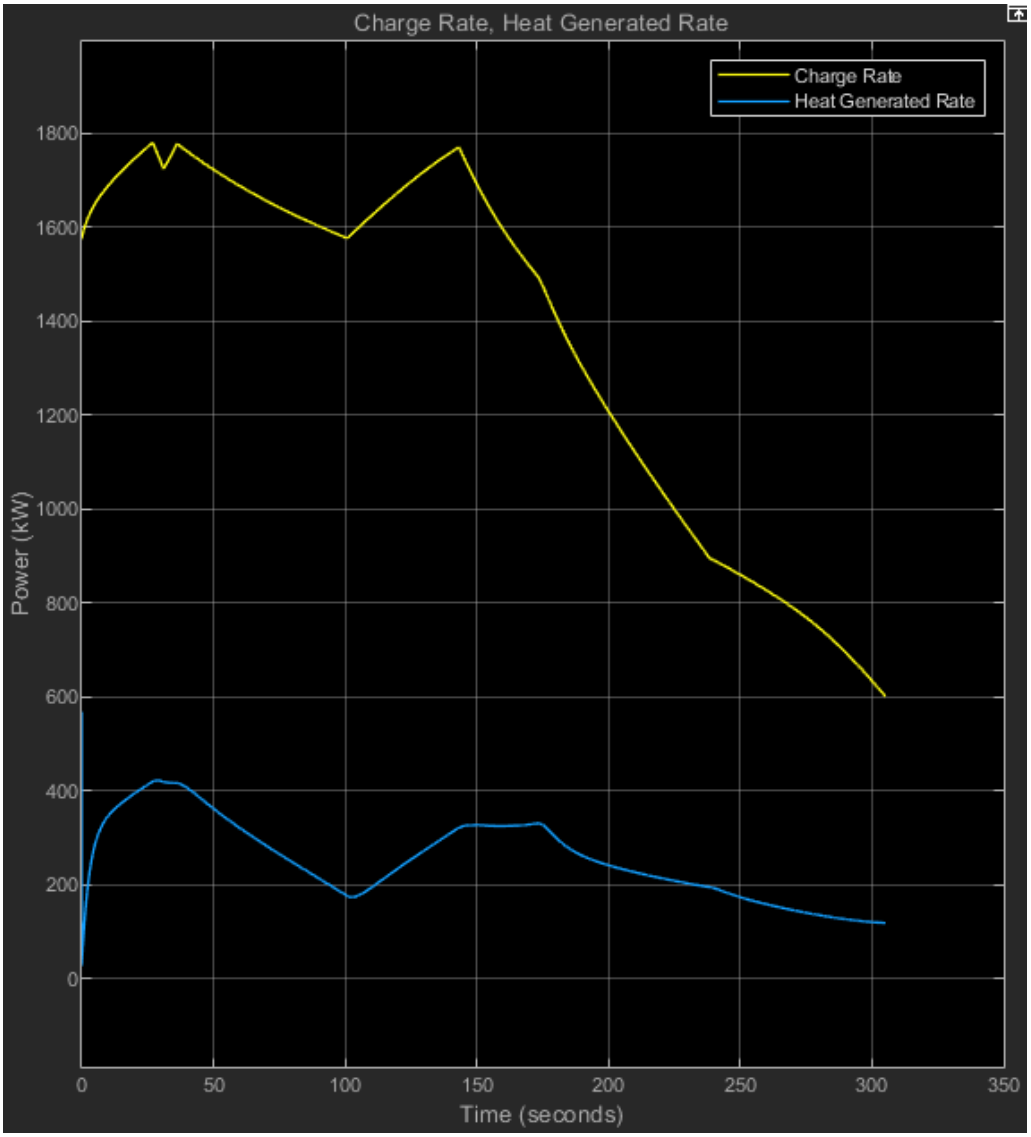

Figure 28: Vehicle level charge rate and heat rate results using a 400V architecture at an outside temperature of 32 Fahrenheit

Figure 28 shows that charge rate decreases quite early in the charge cycle compared to the baseline case shown in Figure 13. This increases the charge time by 50 seconds to 305 seconds versus 255 seconds. However, the heat generated throughout the cycle is relatively similar.

5 Discussion

Experiment	Charge Time (s)	Maximum Cell Temperature (Celsius)	Maximum Wire Temperature (Celsius)	Maximum Rankine Cycle Efficiency (%)
400 V, 20 C	255	35.5	115	15
800 V, 20 C	260	34.5	50	14
400 V, 37 C	250	39	110	18
400 V, 0 C	305	28	105	17.5

Table 1: Overview of results for four experiments

Table 1 compares the results from four experiments shown in section 4. The Simulink model can be used to simulate a wide variety of initial conditions. Therefore, the model's capability is more extensive than the results from these four experiments. These four experiments are used to make comparisons between different architectures and different operating conditions. For the purposes of this analysis, the following paragraphs will explore the trends in each column of Table 1.

5.1 Charging Time

The charge time is not directly a function of the vehicle battery voltage architecture. Since the charging power is set at the cell level to maximize the charge rate without exceeding a charge rate of 15C, the voltage architecture does not decrease the charge rate. Instead, charging is slowed by the lower average cell temperature experienced at 800 V. This lower cell temperature is a result of the decreased fluid temperature from a lower wire heat generation rate. Charge time is much more dependent on the temperature of the battery cell during charging. As the temperature of the cell increases, the resistance of the cell decreases. This leads to more efficient charging at higher temperatures. Over the three charging temperatures of 0° C, 20° C, and 37° C, the higher the average temperature of the cell during charging, the lower the overall charging time. Furthermore, at temperatures below 20° C, the charging time increases significantly from 255 seconds at 20° C to 305 seconds at 0° C. Above 20° C, however, the charging time does not decrease

by the same level. The charging time at 37° C is only 5 seconds shorter than the charging time at 20° C. This is the result of a non-linear relationship between cell temperature and resistance.

5.2 Cell Temperature

Similarly, the maximum cell temperature mostly a function of the ambient temperature. The difference between using a 400 V architecture and an 800 V architecture resulted in a temperature decrease of 1° C. Conversely, the ambient temperature of the system had a greater impact on the maximum temperature of the cell. As the ambient temperature of the cell increased, the temperature of the cell also increased. At 0° C the maximum temperature is 28° C, at 20° C, the maximum temperature is 35.5° C, and at 37° C, the maximum temperature is 39° C. Even at high ambient temperatures, the cell maintains a temperature below 40° C. Above 40° C, lithium ion cells experience accelerated degradation so the results in Table 1 show that this system is successful in controlling the temperature of the cells within a safe range. As the temperature of the coolant increases, the heat dissipation rate also increases because the heat flux is a function of the temperature difference. This effect aids in the cooling of the battery cells at elevated temperatures.

5.3 Wire Temperature

The maximum wire temperature stays within 10° C between 0 to 37° C when using a 400 V architecture. The maximum temperature of the wire reaches 115° C during charging. This temperature is quite high and may be undesirable for safety reasons. Interestingly, the maximum temperature occurs at 30° C, and not at 37° C. This is due to the decreased efficiency of charging at 20° C. The temperature of the wire is time dependent because the temperature of the wire increases throughout the simulation (with the exception of when the current is reduced toward the end of charging). Since the

shortest charge time occurs when the ambient temperature is 37° C, the amount of time when a current is applied to the wire is shortest. This is why the maximum temperature at 37° C is lower than the maximum temperature at 20° C. The temperature of the wire is mostly a function of the voltage architecture since the heat rate is dependent on the current. At 400 V, twice the current is required for the same power output as an 800 V architecture. Table 1 shows that the maximum wire temperature is reduced from 115° C to 50° C when switch from a 400 V to a 800 V architecture. At 50° C, the copper conduit is operating within a safer temperature range. The heat generated by the wire is far greater at 33 kW for a 400 V architecture compared to 8 kW for a 800 V architecture. This leads to a more efficient charge cycle.

5.4 Rankine Cycle Efficiency

Rankine cycle efficiency is a function of the temperature difference between the heat source (the coolant temperature in this case) and the heat sink (the ground or air temperature). Therefore, there is only a 1% difference between the maximum Rankine cycle efficiency as it applies to the 400 V and 800 V architectures. For the 20° C and 37° C cases, the heat sink is set to use the ground temperature of 13° C. Since the efficiency is a function of the temperature difference, there is a greater maximum efficiency of 18% at 37° C versus 15% at 20° C as expected. When the ambient temperature is 0° C, the atmosphere is used as the heat sink as it is colder than the average ground temperature. The creates a maximum efficiency of 17.5% which is similar to the maximum efficiency at 37° C. It should be noted that all of these efficiencies are relatively small. The maximum power generated by the Rankine cycle is only about 50 kW. This value is much smaller than the charging power of approximately 1800 kW.

6 Conclusion

The report above characterizes the performance of a battery thermal management system between an EV and and a charging station. Through four experiments that varied the voltage architecture and ambient temperature, the following conclusions were found.

As the temperature battery cell increases, the charging time decreases. This cell temperature is found to be higher at higher ambient temperatures and lower voltage architectures. Charging time decreased by 50 seconds when the ambient temperature was increased from 0° C to 20° C. In industry, automakers have implemented battery preheating to decrease DC fast charging time [12]. Even at an ambient temperature of 37° C, the temperature of the battery reached a maximum of 39° C. Lithium-ion batteries degrade prematurely above 40° C so this cooling system was successful in controlling the battery's temperature below this threshold.

Increasing the voltage of the battery pack also increases the temperature of the charging cable. The temperature decreased from an unsafe 115° C to a safer 50° C. From this analysis, it is recommended that higher voltage architectures are used to reduce excess heat generation in the charging conductor.

At higher coolant temperatures, Rankine cycle efficiency is higher. R-134a was selected as the working fluid for the organic Rankine cycle due to its frequent use in automotive applications. There are however, significant environmental concerns with the use of R-134a. Accordingly, a less harmful working fluid should be selected. Additionally, with peak efficiencies below 20% it is unlikely that the additional cost of constructing an organic Rankine cycle power plant would outweigh the benefit of energy recuperation.

The main goal of this analysis was to design a system capable of charging an EV with a large 100 kWh battery pack in the same time as a gasoline-powered vehicle through four experiments with varying voltage architectures and ambient temperatures. The average charge time using this system 255 seconds with a maximum charge time of 305 seconds at 0° C. Assuming an average refueling time for an ICE vehicle of 240

seconds. This system is capable of charging the battery pack from 0% to 100% within a minute of an ICE vehicle while maintaining safe battery and charge cable temperatures. This system has the potential to eliminate slow charging times and range anxiety thus increasing the adoption of EVs.

Bibliography

[1] *SAE J1772: Electric Vehicle and Plug in Hybrid Electric Vehicle Conductive Charge Coupler*. Jan. 2010. URL: http://standards.sae.org/j1772_201001/.

[2] Christian Jung. "Power Up with 800-V Systems: The benefits of upgrading voltage power for battery-electric passenger vehicles". In: *IEEE Electrification Magazine* 5 (Mar. 2017), pp. 53–58. DOI: 10.1109/MELE.2016.2644560.

[3] F. Momen, K. Rahman, and Y. Son. "Electrical Propulsion System Design of Chevrolet Bolt Battery Electric Vehicle". In: *IEEE Transactions on Industry Applications* 55.1 (2019), pp. 376–384. DOI: 10.1109/TIA.2018.2868280.

[4] K. Zaghib et al. "Safe and fast-charging Li-ion battery with long shelf life for power applications". In: *Journal of Power Sources* 196.8 (2011), pp. 3949–3954. ISSN: 0378-7753. DOI: https://doi.org/10.1016/j.jpowsour.2010.11.093. URL: http://www.sciencedirect.com/science/article/pii/S0378775310020847.

[5] T. Huria et al. "High fidelity electrical model with thermal dependence for characterization and simulation of high power lithium battery cells". In: *2012 IEEE International Electric Vehicle Conference*. 2012, pp. 1–8. DOI: 10.1109/IEVC.2012.6183271.

[6] Anna Tomaszewska et al. "Lithium-ion battery fast charging: A review". In: *eTransportation* 1 (2019), p. 100011. ISSN: 2590-1168. DOI: https://doi.org/10.1016/j.etran.2019.100011. URL: http://www.sciencedirect.com/science/article/pii/S2590116819300116.

[7] Jason B. Quinn et al. "Energy Density of Cylindrical Li-Ion Cells: A Comparison of Commercial 18650 to the 21700 Cells". In: *Journal of The Electrochemical Society* 165.14 (2018), A3284–A3291. DOI: 10.1149/2.0281814jes. URL: https://doi.org/10.1149%2F2.0281814jes.

[8] MATLAB. *version R2020b*. Natick, Massachusetts: The MathWorks Inc., 2020.

[9] S. W. Churchill and M. Bernstein. "A Correlating Equation for Forced Convection From Gases and Liquids to a Circular Cylinder in Crossflow". In: *Journal of Heat Transfer* 99.2 (May 1977), pp. 300–306. ISSN: 0022-1481. DOI: 10.1115/1.3450685. eprint: https://asmedigitalcollection.asme.org/heattransfer/article-pdf/99/2/300/5909086/300_1.pdf. URL: https://doi.org/10.1115/1.3450685.

[10] J.H. Dellinger. "The temperature coefficient of resistance of copper". In: *Journal of the Franklin Institute* 170.3 (1910), pp. 213–216. ISSN: 0016-0032. DOI: https://doi.org/10.1016/S0016-0032(10)90872-7. URL: http://www.sciencedirect.com/science/article/pii/S0016003210908727.

[11] Eric W. Lemmon, M. L. Huber, and M. O. McLinden. *NIST Standard Reference Database 23: Reference Fluid Thermodynamic and Transport Properties - REFPROP*. 10.0. National Institute of Standards and Technology, Standard Reference Data Program. Gaithersburg, 2018. URL: http://www.nist.gov/srd/nist23.cfm.

[12] Zhiguo LEI et al. "Preheating method of lithium-ion batteries in an electric vehicle". In: *Journal of Modern Power Systems and Clean Energy* 3.2 (June 2015), pp. 289–296. ISSN: 2196-5420. DOI: 10.1007/s40565-015-0115-1. URL: https://doi.org/10.1007/s40565-015-0115-1.

A Rankine Cycle MATLAB Code

```
%Import REFPROP data
m=100;
n=100;
fluidTables = twoPhaseFluidTables([80,500],[.001,7],m,m,n,...
'R134a','C:\Users\mcele\OneDrive - Washington University in St. ...
    Louis\Backup7-17-19\Programs\REFPROP');
T_liquid=fluidTables.liquid.T;
s_liquid=fluidTables.liquid.s;
p_liquid=fluidTables.p;
T_vapor=fluidTables.vapor.T;
s_vapor=fluidTables.vapor.s;
p_vapor=fluidTables.p;
T_sat=[];

%Find Saturation points
for i=1:n
    Tl_sat(i,2)=T_liquid(m,i);
    Tl_sat(i,1)=s_liquid(m,i);
    Tl_sat(i,3)=p_liquid(i);
end
for i=1:n
    Tv_sat(i,2)=T_vapor(1,i);
    Tv_sat(i,1)=s_vapor(1,i);
    Tv_sat(i,3)=p_vapor(i);
end

%Plot T-s diagram
hold on
% plot(fluidTables.liquid.s,fluidTables.liquid.T)
% plot(fluidTables.vapor.s,fluidTables.vapor.T)
plot(Tl_sat(:,1),Tl_sat(:,2));
```

```
31 plot(Tv_sat(:,1),Tv_sat(:,2));
32 hold off
33
34
35 %In and out temperatures
36 Thigh=350;
37 Tlow=286;
38
39 %State Calculations
40 %State 1
41 T1=Tlow;
42 T_row=0;
43 for i=1:m
44     if Tl_sat(i,2) ≥ T1
45         T_row=i;
46         break
47     end
48 end
49 S1=Tl_sat(T_row,1);
50 P1=Tl_sat(T_row,3);
51
52 %State 4
53 T4=T1;
54 T_row=0;
55 for i=1:m
56     if Tv_sat(i,2) ≥ T1
57         T_row=i;
58         break
59     end
60 end
61 S4=Tv_sat(T_row,1);
62 P4=P1;
63
```

```
%State 3
T3=Thigh;
S3=S4;
target_t_below = 0;
target_t_below_p = 0;
for p_index=1:n
    target_index = 0;
    for s_row=1:m
        s_test=s_vapor(s_row,p_index);
        if s_test≥S4
            target_index = s_row;
            break
        end
    end
    if target_index ≥ 1
        t_test=T_vapor(target_index,p_index);
        if t_test > target_t_below & t_test ≤ T3
            target_t_below = t_test;
            target_t_below_p = p_index;
        end
    end
end
P3=fluidTables.p(target_t_below_p);

%State 2
P2=P3;
S2=S1;
target_index=0;
for s_row=1:m
    s_test=s_liquid(s_row,target_t_below_p);
        if s_test≥S2
            target_index = s_row;
            break
```

```
97          end
98  end
99  T2=fluidTables.liquid.T(target_index,target_t_below_p);
100
101 %Calculate enthalpies (kJ/kg)
102 H1=S1*T1;
103 H2=S2*T2;
104 H3=S3*T3;
105 H4=S4*T4;
106
107 %Calculate Heat and Work Flows (kJ/kg)
108 W_pump=H2-H1
109 Q_in=H3-H2
110 W_turbine=H3-H4
111 Q_out=H3-H2
112
113 efficiency=(W_turbine-W_pump)/Q_in
```